Title

On the use of Nafion® in electrochemical studies of carbon supported oxygen reduction catalysts in aqueous media

Journal

Journal of Electroanalytical Chemistry, 780

Authors

Chlistunoff, Jerzy
Sansiñena, José-María

Publication Date

2016-09-14

Peer reviewed

Journal of Electroanalytical Chemistry 780 (2016) 134–146

Contents lists available at ScienceDirect

Journal of Electroanalytical Chemistry

journal homepage: www.elsevier.com/locate/jelechem

On the use of Nafion® in electrochemical studies of carbon supported oxygen reduction catalysts in aqueous media

Jerzy Chlistunoff *, José-María Sansiñena

Los Alamos National Laboratory, P.O. Box 1663, Los Alamos, NM 87545, USA

ARTICLE INFO

Article history:
Received 12 April 2016
Received in revised form 16 August 2016
Accepted 12 September 2016
Available online 14 September 2016

Keywords:
Self-assembly
Graphitic
Catalyst support
Hydrophobicity
RDE

ABSTRACT

The paper presents the results of a voltammetric and rotating ring disk electrode (RRDE) study of oxygen reduction reaction (ORR) catalyzed by Fe and Co porphyrins and phthalocyanines adsorbed on a high surface area carbon (Vulcan XC72) and by carbon supported Pt catalysts in presence of various quantities of Nafion®. The results demonstrate that the hydrophobic backbone of Nafion® self assembles on nanoparticles of common carbon supports of ORR catalysts. The phenomenon is promoted by the attractive interactions of the backbone with the graphitic surfaces of carbon particles. It leads to a significant ORR inhibition as a result of the spillover of the hydrophobic Nafion® component onto the catalyst particles. The extent of the inhibition depends on the type and the amount of the catalyst on the carbon surface and the degree of carbon surface graphitization. The activity of the transition metal macrocycles is suppressed by up to two orders of magnitude, whereas that of low Pt loading (4.8%) catalysts by less than one order of magnitude. The results demonstrate a great risk of incorrect catalyst activity determinations when using even very small Nafion® quantities as the catalyst ink dispersing agent.

1. Introduction

Nafion® is a polymer electrolyte commonly used in proton exchange membrane fuel cells (PEMFCs). It has a hydrophobic perfluorinated backbone, whereas its side chains are outfitted with strongly acidic sulfonic groups responsible for providing proton conductivity [1]. Bulk Nafion® is phase separated, i.e., its backbone forms hydrophobic, whereas the sulfonic groups hydrophilic domains. The hydrophilic domains are capable of conducting hydrated protons and provide environment, where hydrogen oxidation reaction (HOR, fuel cell anode) and oxygen reduction reaction (ORR, fuel cell cathode) can occur in presence of suitable electrocatalysts. The phase separation of the ionomer enables the formation of a continuous network of ion conducting channels, but it also eliminates some catalyst particles from the participation in the electrode reactions, when they contact ionically non-conductive, i.e., hydrophobic parts of the ionomer.

The incomplete catalyst utilization in fuel cells can be expected just from the statistical distribution of the catalyst particles and the respective domains in the polyelectrolyte [2]. However, the interactions between the dispersed but bulk catalyst and Nafion® quantities are more complex, as extensively documented in literature [2–10]. The phenomenon is a serious concern for the cathode process (ORR) due to the sluggishness of the reaction [11,12] and the limited and largely monopolized resources of platinum, which is the major component of the best known ORR catalysts. In consequence, an extensive research aimed at the development of novel cathode catalysts has been conducted. The effort is directed towards either lowering the Pt loading necessary for the effective catalysis or replacing Pt (or other precious metals) with new materials. Among the latter, some of the most promising are pyrolyzed Fe/N/C composites [11–13]. Their postulated active site structure [12,13] is very similar to that in macrocyclic complexes known to be catalytically active in ORR, such as iron or cobalt porphyrins, phthalocyanines, and corroles [14–18]. Different active centers in the Fe/N/C composites and Pt based promote different ORR mechanisms [12,16,19–22].

The potential suitability of any new ORR catalyst for fuel cell applications is examined using numerous characterization techniques. Most importantly, the catalyst activity is first tested in aqueous electrolytes. Typically, the testing involves rotating disk (RDE) or rotating ring disk (RRDE) electrode measurements in acidic ($HClO_4$ or H_2SO_4) electrolytes. The measurements can determine the intrinsic activity of a catalyst and its selectivity for the desired four electron reduction of O_2 to water compared to that leading to hydrogen peroxide (two electron reduction). The rotating electrode technique has become the primary way of screening new catalysts. As the intrinsic activities of newly developed materials are decisive in determining their potential as practical ORR catalysts, it is important that correct procedures are used in the activity determinations. In order to minimize competition and/or shielding effects between the catalyst particles, the catalyst is first deposited onto a high surface area conducting support, e.g., carbon Vulcan XC72. Afterwards, a catalyst ink is fabricated by dispersing the supported catalyst in a suitable solvent and a small volume of the ink is deposited onto the (typically glassy carbon) disk of an RDE (RRDE) and evaporated. The catalyst layer has to be uniform and entirely cover the disk electrode

* Corresponding author.
E-mail address: jerzy@lanl.gov (J. Chlistunoff).

http://dx.doi.org/10.1016/j.jelechem.2016.09.014
1572-6657/

to provide well defined hydrodynamic conditions, essential for the correct determination of the reaction rate and selectivity [23]. Among others, in order to achieve this goal, the catalyst ink must be well dispersed and durable, i.e., it should not settle or clump. Nafion® is frequently added to catalyst inks to improve the catalyst dispersion and the catalyst layer integrity and uniformity [23]. The amount of Nafion® used as the ink dispersing agent in novel catalyst studies is arbitrarily chosen. In accordance with the intended role of the ionomer, its content in the catalyst layer is typically below 20% by weight [14,24–26], i.e., enough to produce the desired surface effect but well below to fill the voids between the support particles and create bulk polymer phase. In some studies, however, the quantities as high as 33% [27], 49% [28], 53% [29] and 56% [30] were used. Such Nafion® amounts are closer to those in PEMFCs and may have had similar effects to those reported for fuel cell Pt catalyst layers [3,6,7,10,31–35].

As the alternative ORR catalysts have not yet reached the required mass/volume activity to be employed in practical PEMFCs, studies of Nafion® effects on their performance are missing. The small Nafion® amounts required to prepare well dispersed catalyst inks for RDE studies are likely believed to be insufficient to block a meaningful fraction of the catalyst particles. Likewise, any bulk Nafion® potentially present in the catalyst layer might be considered harmless due to the open morphology of its surface in presence of liquid water [36]. However, the ability of Nafion® to act as a surfactant indicates the existence of specific interactions between the catalyst/support particles and the ionomer. In fact, a strong monolayer Nafion® adsorption from liquid solutions on a variety of carbon supported Pt catalysts and catalyst supports has been demonstrated [37–41]. While the respective catalyst activities have not been reported [37–40], the voltammograms of carbon nanotube (CNT) supported Pt catalysts in Ref. [40] clearly demonstrate a significant Nafion® induced decrease in Pt/CNT electrochemically active surface area. This suggests that Nafion® adsorption present in solution also persists in solid catalyst layers and can potentially affect the measured catalyst activities. In this manuscript we will demonstrate that the above supposition is fully justified for at least two different classes of carbon supported catalysts: low loading Pt catalysts and transition metal porphyrins and phthalocyanines. The latter have been extensively studied as ORR catalysts and can also act as models for the pyrolyzed Fe/N/C composites [11–13].

2. Experimental

The following macrocyclic complexes were obtained from Aldrich and used as received: Iron (III) tetraphenylporphyrin chloride (5,10,15,20-Tetraphenyl-21*H*,23*H*-porphine iron(III) chloride, >94%, hereafter called FeTPPCl), iron(III) phthalocyanine chloride (~95%, hereafter called FePCCl), iron(III) octaethylporphyrin chloride (2,3,7,8,12,13,17,18-octaethyl-21*H*,23*H*-porphine iron(III) chloride, hereafter called FeOEPCl), cobalt(II) phthalocyanine (97%, hereafter called CoPC), cobalt(II) tetramethoxyphenylporphyrin (5,10,15,20-tetrakis(4-methoxyphenyl)-21*H*,23*H*-porphine cobalt(II), 97%, hereafter called CoTMeOPP), cobalt(II) octaethylporphyrin (2,3,7,8,12,13,17,18-Octaethyl-21*H*,23*H*-porphine cobalt(II), hereafter called CoOEP), cobalt(II) tetraphenylporphyrin (5,10,15,20-Tetraphenyl-21*H*,23*H*-porphine cobalt(II), 85%, hereafter called CoTPP).

Anhydrous dichloromethane (DCM, ≥99.8% with 50–150 ppm amylene as stabilizer, Sigma Aldrich), Vulcan XC72, a high surface area (~240 $m^2\ g^{-1}$) carbon (Cabot) were used as received.

All experiments were performed using 0.5 mol dm^{-3} H_2SO_4 at 25 °C as the background electrolyte. The electrolyte was prepared using a commercial sulfuric acid (Certified ACS Plus, Fisher Chemical) and Millipore® water.

Highly ordered pyrolitic graphite (HOPG) grade SPI-2 from SPI Supplies (7 mm × 7 mm × 1 mm platelet, mosaic angle 0.8° ± 0.2°, the lateral grain size up to 0.5–1 mm) was used as received.

The working electrode in RRDE experiments was a Pine model AFE7R9GCPT electrode with a glassy carbon disk and a Pt ring. Its nominal collection efficiency of 37% was confirmed by independent measurements using $K_3Fe(CN)_6$ in KCl solutions. In some voltammetric experiments a 3 mm glassy carbon disk electrode (Bioanalytical Systems) was used.

Voltammetric HOPG electrodes (~4.8 mm diameter) were prepared using a procedure described in Supplementary information.

The counter electrode in all experiments was a graphite rod, whereas the reference electrode was a hydrogen electrode utilizing 6% H_2 in Ar in equilibrium with Pt black coated platinum wire immersed in 0.5 mol dm^{-3} H_2SO_4. The equilibrium potential of the reference electrode at Los Alamos elevation (2100 m) is 39 mV positive than the potential of a reversible hydrogen electrode (RHE) in the respective solution at the sea level.

In all RRDE experiments, the first scan was cathodic and the final potential was equal to the initial potential irrespective of the number of individual scans performed. The experiments were performed using electrode rotation rates ≥400 rpm and a scan rate of 10 mV s^{-1}. The ring potential was held at +1.24 V vs. RHE to assure transport controlled oxidation of hydrogen peroxide generated in ORR. All voltammograms in kinetic analysis were corrected for the respective background currents measured in oxygen free solutions under the identical conditions. The background corrected currents (i_{corr}) were subsequently used to calculate the respective kinetic currents (i_k) using standard mass transfer correction: $i_k = i_{corr} i_L / (i_L - i_{corr})$, where i_L stands for the limiting ORR current.

In order to accurately determine electrochemical surface properties of the catalysts deposited onto the RRDE, multi-cycle voltammograms in oxygen free atmosphere were recorded at significantly higher scan rates (100–1000 mV s^{-1}). The voltammograms (and the capacitive currents extracted from them) reported in the paper were obtained from the second voltammetric cycles, which were not affected by uncontrolled electrode hold at the open circuit potential.

Two extensively characterized [42–46] commercial Pt catalysts supported on Vulcan were used in the study: 20% Pt (BASF) and 4.8% Pt (TEC10V05E, Tanaka Kikinzoku Kogyo). The third studied Pt (4.8%) catalyst was supported on graphitized carbon. Its properties were not disclosed by the manufacturer. The necessary X-ray diffraction and BET measurements were performed by the authors of the paper. The respective numbers are 157 $m^2\ g^{-1}$ for the BET surface area and 4.8 nm for the average Pt particle size as determined from the Scherrer equation [47]. For simplicity, the three Pt catalysts will be hereafter called Pt20V (20% BASF), Pt4.8V (4.8% Tanaka), and Pt4.8G (Pt on graphitized support), respectively.

The catalyst inks for macrocyclic ORR catalysts were prepared using the following procedure. Around 40 mg of Vulcan XC72 were mixed with a few milligrams of the desired macrocycle and 2–4 cm^3 of DCM and slowly sonicated to dryness. Afterwards, the dry residue was sonicated for around 1 h with 8 cm^3 of isopropanol (IPA) and small quantities of 5% Nafion® solution (Ion Power, Inc.). The inks of Pt catalysts and of pure XC72 carbon were prepared by directly mixing the solids with IPA and Nafion® followed by sonication. The amount of 5% Nafion® solution used to prepare the catalyst inks varied from 0 to 2.7 μl per 1 mg of the carbon support and was found to be an important parameter determining the extent of ORR inhibition for various catalysts. The ratio of the volume (μl) of 5% Nafion® solution to the weight (mg) of carbon support used for the catalyst ink preparation will be denoted by R, where R = 1 corresponds to 1 μl of the 5% Nafion® solution used for 1 mg of the carbon support, which is equivalent to 46.8 μg of pure Nafion® per 1 mg of the support. The inks of Pt catalysts were prepared in a similar way, i.e., a catalyst sample of ~40 mg was dispersed by sonication in 8 cm^3 of IPA with small Nafion® addition. As with the non-precious catalysts, the Nafion® content in those inks is hereafter expressed by the parameter R. All inks were stored in tightly closed glass vials at room temperature.

A Pine Instruments bipotentiostat model AFCBP1 controlled by Aftermath software (Pine Instruments) was used for all rotating ring disk experiments. Unless otherwise stated, all experiments were performed for a constant total loading of 0.1 mg of the carbonaceous support, which corresponded to ~0.4 mg_{carbon} cm^{-2}_{disk}. The deposition of the ink on the glassy carbon disk of the RRDE and its evaporation were monitored under a microscope.

3. Results

3.1. The effect of Nafion on the electrochemical behavior of Vulcan XC72

With its high specific surface area of ~240 m^2 g^{-1}, Vulcan XC72 significantly contributes to the overall surface area of catalysts utilizing it as the support. Additionally, its interactions with Nafion® may alter the way the ionomer interacts with the catalyst particles. Consequently, the first part of our research was devoted exclusively to Vulcan XC72, which was the catalyst support in all but one (Pt4.8G) of the studied catalysts. Cyclic voltammograms were recorded for Vulcan XC72 inks containing from 0 to 1.5 μl of 5% Nafion® per 1 mg of carbon ($0 \le R \le 1.5$) in deoxygenated H_2SO_4 solutions at various scan rates ranging from 100 mV s^{-1} (Fig. 1) to 1000 mV s^{-1}. The measured currents were proportional to the scan rate, i.e., exhibited capacitive character in the entire potential range applied (0.04–0.74 V vs. RHE). They were virtually independent of Nafion® concentration for $R \le 0.6$. However, when R increased to 0.9 and above ($0.9 < R \le 1.5$), the measured currents dropped to <20% and 10% of their initial values, respectively (Fig. 1). The suppressed currents still exhibited purely capacitive character. The changes in the capacitive currents demonstrate Nafion® adsorption on the carbon surface. The adsorption was reversible, i.e., the capacitive currents increased exactly as expected from Fig. 1 when R decreased to 0.3 through additions of Vulcan XC72 and IPA to the ink and its brief sonication. The reversibility of the Nafion® adsorption indicates a physical character of the interactions (i.e., lack of bond formation) between the ionomer and the carbon surface.

The extent of Nafion® adsorption can be inferred from the measured capacitive (double layer charging) currents (i_{dl}). The charging current is proportional to the differential double layer capacity of both Nafion® covered ($C_{dl,Nafion®}$) and free ($C_{dl,free}$) carbon surface:

$$i_{dl} = (C_{dl,free}(1-\Theta) + C_{dl,Nafion®}\Theta)A_{real}v \quad (1)$$

where A_{real} is the real surface area of the carbon deposited on the disk, v is the scan rate, whereas Θ is the surface coverage by Nafion®. Eq. (1) neglects the contribution from the glassy carbon disk, whose surface area (~0.25 cm^2) is significantly lower than that of the XC72 (nominally 240 cm^2). The equation was used to calculate the surface coverages of the carbon surface by Nafion® for different Nafion® concentrations. In the calculations, the currents measured for the ink containing no Nafion® were identified with no surface coverage ($\Theta = 0$), whereas the currents measured for R = 1.5 were assumed to correspond to $\Theta = 1$ (maximum surface coverage) based on the observed flattening of the i_{dl} vs. R dependence at high Nafion® contents (inset in Fig. 1).

The observed decrease in the capacitive currents (Fig. 1) indicates that the adsorption of Nafion® occurs through its hydrophobic component. In similarity to neutral organic molecules adsorbed on electrodes in aqueous media [48], the perfluorinated backbone of the ionomer shifts the ionic component of the electrical double layer away from the conducting carbon surface and acts as a thick layer of low dielectric permittivity material in a capacitor, i.e., lowers the double layer capacity.

The values of Θ obtained from Eq. 1 were used to calculate the ratio of the surface area covered by Nafion® to that uncovered ($\Theta/(1-\Theta)$) to obtain Nafion® "adsorption isotherm" (Fig. 2). The real adsorption isotherm could not be determined from the present data, because the equilibrium concentrations of Nafion® in the inks corresponding to the measured surface coverage were unknown. They likely corresponded to unknown equilibrium states that were "frozen" at a later stage of the evaporation process due to the limited mobility of the large ionomer molecules between the already closely packed carbon particles.

The concave shape of the "adsorption isotherm" is consistent with the presence of attractive interactions in the adsorbed layer and/or repulsive interactions in the solution phase and implies a self-assembly character of the adsorption. In absence of such interactions, the

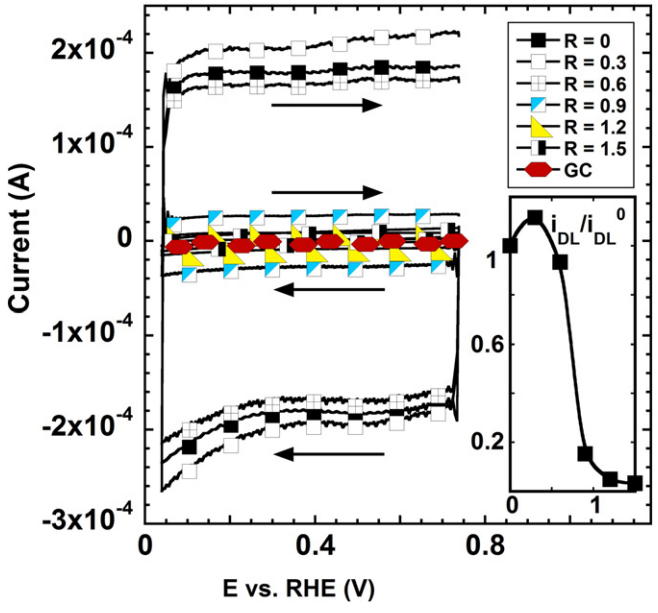

Fig. 1. Capacitive voltammetric currents measured for 0.1 mg of Vulcan XC72 mixed with various quantities of 5% Nafion® solution. Scan rate 100 mV s^{-1}. The ratio of the capacitive currents at 0.3 V for various Nafion® contents (i_{DL}) to that measured in absence of Nafion® (i^0_{DL}) is plotted against R in the inset. The currents used to create the graph in the inset were averages of the absolute currents measured at 0.3 V in both forward and reverse scans.

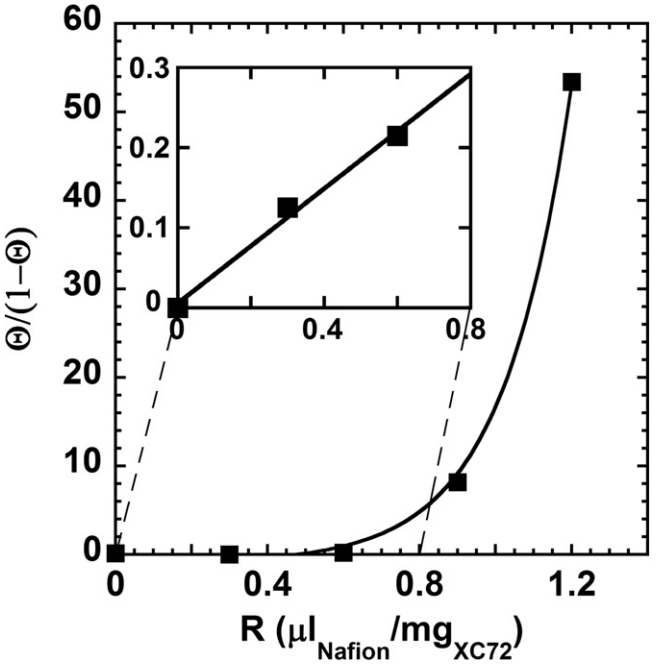

Fig. 2. Calculated (Eq. 1) ratio of surface areas of Vulcan XC72 covered with Nafion® and not covered plotted versus Nafion® content (R) in the ink.

adsorption would be described by Langmuir isotherm, which predicts a straight linear increase in $\Theta/(1-\Theta)$ with Nafion® concentration [49]. The self-assembly hypothesis seems to remain at odds with the conclusion reached by Ma et al. [37] and by Ma Andersen et al. [38] that Nafion® adsorption on Vulcan from low concentrated aqueous solutions is governed by the Langmuir isotherm. In principle, different solvents used by the authors of references [37,38] (water) and by us (IPA) might be responsible for this discrepancy. However, Nafion® molecules are complex entities, which participate in a variety of interactions involving their polar (ether and sulfonic) and non-polar (perfluorinated backbone) groups. The previous papers [37,38,41] reported actual Nafion® quantities on the Vulcan surface in presence of ionomer's liquid solutions. To the contrary, the voltammetric technique used in our study (Fig. 1) senses almost exclusively the presence of the hydrophobic Nafion® component on the surface in absence of liquid solution.

Furthermore, the studies of Nafion® adsorption on Vulcan by Ma et al. [37] and Ma Andersen et al. [38] demonstrate that the monolayer surface coverage of the ionomer corresponds to $R \approx 2.0$ [37] and $R \approx 2.1$ [38], respectively, using our nomenclature. At the same time, our data (Fig. 1) indicate that the maximum surface coverage of Vulcan by the hydrophobic component of Nafion® corresponds to a lower R (≥1.5). Quite likely, if higher Nafion® concentrations were used in the previous studies [37,38], an adsorption hysteresis consistent with a concentration driven phase transitions from the Langmuir adsorption involving the hydrophobic and hydrophilic Nafion® components to a two dimensional solid (self-assembly involving hydrophobic Nafion® backbone only) and vice versa could be observed. Interestingly, Cherstiouk et al. [41] reported a monolayer Nafion® surface coverage of Vulcan in IPA-water (3:2) mixtures corresponding to our $R \approx 1.3$. Unfortunately, no adsorption isotherm was presented in Ref. [41].

While the self-assembly of Nafion® was most likely not yet present in our Vulcan inks in liquid state, its predecessor, i.e., Langmuir adsorption [37,38] was already taking place and was largely involving the hydrophobic backbone of Nafion® as indicated by the observed ink dispersion behavior. The inks with R ≤ 0.6, whose electrochemical behavior was virtually unaffected by Nafion® (Fig. 1), flocculated a short time after the sonication, irrespective of the sonication time. On the other hand, the inks with R ≥ 0.9 were easily dispersed, stable for long periods and their respective double layer currents were significantly suppressed (Fig. 1). The adsorption predominantly involving the hydrophobic Nafion® component eliminates its repulsive interactions with the hydrophilic solvent but preserves the attractive interactions between the hydrophilic component and the solvent. The resultant micelle-like structures with the predominantly hydrophobic core (carbon + Nafion® backbone) and hydrophilic and partially dissociated shell (Nafion® ether + sulfonic groups) prevent carbon particles from agglomeration.

In conclusion, both hydrophobic and hydrophilic Nafion® components contribute to its adsorption on Vulcan in liquid media. However, the self-assembly becomes the predominant, if not the only, adsorption mode at higher Nafion® concentrations, which are attained during the ink evaporation. These concentrations are most likely higher than the maximum Nafion® concentrations (~2 g dm^{-3}) used in the previous studies [37,38], which demonstrated the Langmuirian character of the Nafion® adsorption on Vulcan.

While the observed ~95% decrease in the Vulcan capacitive currents originating from the self-assembly of Nafion® is consistent with virtually 100% surface coverage by the ionomer (the double layer capacity is never zero), it does not exclude additional Nafion® accumulation on top of its self-assembled layer. For that reason, we performed simple calculations of the Nafion® layer thickness from the Nafion® quantity (R = 1.5) corresponding to the maximum observed surface coverage. Because of the structural complexity of Nafion® molecules, various options were considered. Within the first approximation (hereafter called A_{BET}), it was assumed that Nafion® molecules are sufficiently flexible to adjust to all morphological features of carbon particles (BET area of 240 $m^2\ g^{-1}$ was used). In the second approximation (called $A_{spherical}$), it was assumed that Nafion® molecules can effectively adsorb on spherically shaped particles and are unable to adjust to their morphological features (an average carbon particle diameter of 30 nm was used [44]). Two variations were considered within each approximation. In the first variation ($V_{complete}$), it was assumed that entire Nafion® molecules participated in the compact layer formation and thus contributed to its thickness (Nafion® density of 2.075 g cm^{-3} was used). In the second variation ($V_{backbone}$), it was assumed that only the hydrophobic backbone of the ionomer created the compact layer, whereas the side chains were dangling outside. In that case, the density of Teflon (2.2 g cm^{-3}) and a molecular mass of Nafion® monomer reduced by the mass of its side chain were used to calculate the thickness. The following results were obtained for the above combinations: $A_{BET}V_{complete}$ – 0.15 nm; $A_{BET}V_{backbone}$ – 0.095 nm; $A_{spherical}V_{complete}$ – 0.41 nm; $A_{spherical}V_{backbone}$ – 0.26 nm. These numbers can be compared with relevant dimensions of Nafion® molecules, such as the length of CF bond (0.13–0.14 nm in various perfluorinated hydrocarbons) or the diameter of its backbone (0.32 nm from the cylindrical diameter of C_2F_6 molecule or 0.34 nm from the density of teflon). The above comparison leaves little doubt that no more than a single monolayer of Nafion® is adsorbed on Vulcan at R = 1.5 (full surface coverage from the double layer charging currents in Fig. 1). As could be expected, the above data also demonstrate that Nafion® molecules cannot adjust to all microscopic features of carbon particles and it is rather the average size of the particles than their BET surface area that determines the quantity of adsorbed Nafion®.

A comment may be expected on the state of Nafion® in the studied layers, when its concentration is too low to start the self-assembly (R ≤ 0.6) or after the self-assembly completed (1.9 ≥ R > 1.5). Two major scenarios are possible. The ionomer may exist as either individual molecules (most likely adsorbed for R ≤ 0.6) or as clusters similar to those observed by Lopez-Haro and coworkers [50]. We found that the expected quantity of such clusters would be around an order of magnitude (7–14 times) lower than the lowest quantity observed by the authors of Ref. [50]. As will be demonstrated in the forthcoming sections, Nafion® present as isolated molecules or aggregates in such quantities has virtually no effect on the activity of the studied catalysts.

3.2. The effect of Nafion® on the electrochemical behavior of graphitic (HOPG) and disorganized (GC) carbon surfaces

That the self-assembly of Nafion® on Vulcan occurs through the ionomer's hydrophobic component suggests that it is predominantly promoted by the Vulcan's graphitic surfaces, which markedly contribute to its overall surface area [51,52]. This hypothesis is supported by recent molecular dynamics (MD) study [53] as well as by the fact that Nafion® self-assembles on highly oriented pyrolytic graphite (HOPG), as demonstrated by Masuda et al. [54].

A number of experiments were performed in our study to evaluate the effects of graphitic and disorganized carbon surfaces on Nafion® self-assembly. We were not able to promote self-assembly of the ionomer on either GC or HOPG surfaces from its aqueous or mixed H_2O + IPA H_2SO_4 solution (see Supplementary information). However, a clear difference between the affinities of Nafion® to disorganized (GC) and graphitic (HOPG) carbon surfaces was demonstrated for solution cast Nafion® films. The films were fabricated through the deposition of 10 μl aliquots of a Nafion® solution obtained by 50-fold dilution of its commercial (5%) solution with IPA followed by a brief drying in air. While the presence of Nafion® film (confirmed before and after the electrochemical experiments) had virtually no effect on the capacitive currents of GC, the surface of HOPG was found severely blocked (Fig. 3).

The effect of Nafion® on the electrical double layer of HOPG (Fig. 3) is consistent with Nafion® self-assembly [54] promoted by the attractive interactions between its hydrophobic component and the ordered and hydrophobic graphitic surfaces of HOPG. The lack of Nafion® self-

assembly on flat HOPG surfaces in presence of liquid (electrolyte) phase does not contradict the above conclusion. A significant negative entropy change can be expected for Nafion® self-assembly on virtually atomically flat HOPG surfaces [54]. A similar effect is much less important for relatively small (~30 nm) Vulcan particles [44], where no concerted alignment of multiple Nafion strands is necessary. Each of such particles can be virtually encircled by a single Nafion® strand, whose length can vary from ~200 nm to ~2000 nm, as estimated from the reported average molecular weight of the polymer [1].

The complete lack of Nafion® self-assembly on GC can be linked to the disorganized morphology of its surface. In similarity to HOPG, carbon atoms in GC are also sp^2 hybridized, but form a randomly distributed network of fullerene-like structures [55]. In consequence, a polished surface of the material exhibits an "amorphous" character and significantly lower hydrophobicity, which cannot promote strong interactions with the hydrophobic component of the ionomer.

The demonstrated strong hydrophobic interactions between the polymer backbone and graphitic surfaces make us believe that such graphitic domains of Vulcan are predominantly responsible for the self-assembly of Nafion® on its surface. However, the measured capacitive currents (Fig. 1) reflect the overall change in the double layer capacity of both graphitic and "amorphous" surface domains of Vulcan and demonstrate that the entire Vulcan surface is covered by Nafion at R = 1.5. In spite of the lack of strong attractive interactions between Nafion® backbone and "amorphous" carbon surfaces (Fig. 3), the orientation of Nafion® molecules over such domains in Vulcan is imposed by the strong interactions between the backbone and the neighboring graphitic surface domains.

3.3. Preliminary studies of Co and Fe macrocycles as probes to study Nafion® effects on the kinetics of ORR

While numerous macrocyclic complexes catalyze ORR, not all of them were expected to meet the criteria of stability and mechanism simplicity to guarantee their use to evaluate Nafion® effects on the ORR kinetics. We found that the Nafion® free inks of all selected Vulcan supported porphyrins and phthalocyanines flocculated immediately after sonication. Addition of Nafion® facilitated the catalyst dispersion in the inks. The lowest quantity of Nafion® that somewhat reduced the ink flocculation corresponded to R = 0.3. Such amount of the ionomer did not result in its self-assembly on pure Vulcan and was

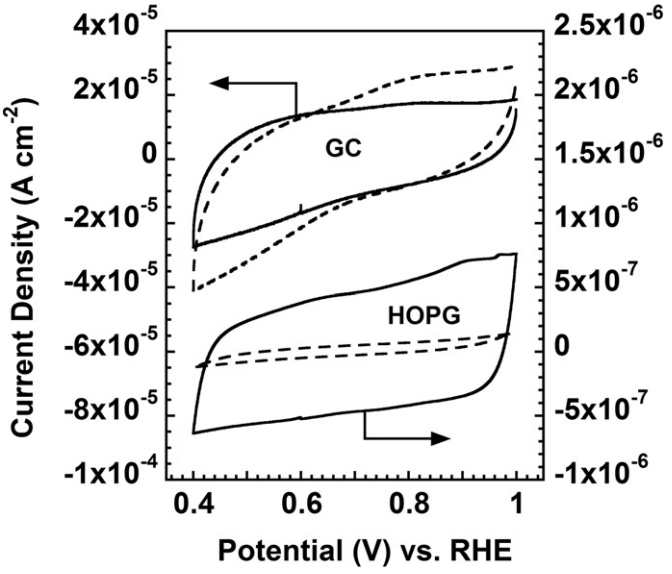

Fig. 3. Capacitive voltammetric current densities measured for a 3 mm glassy carbon disk and a 4.8 mm HOPG electrode in 0.5 mol dm^{-3} sulfuric acid before (solid lines) and after depositing Nafion® film (see text). Scan rate 100 mV s^{-1}.

selected as the lowest Nafion® quantity for the preliminary studies. However, even for R = 0.3, it was impossible to evenly spread the catalyst over the entire disk surface, unless large catalyst quantities were applied. The lowest catalyst loading guaranteeing a barely acceptable quality of the catalyst layer corresponded to ~0.4 mg cm^{-2}. The estimated catalyst layer thickness for such a loading is ~1.8 μm and significantly exceeds the maximum thickness for carbon supported Pt catalyst layers [56], which allows for accurate catalyst activity determination [56–58] from RDE voltammetry, especially at high current densities. In thicker catalyst layers, oxygen transport can be impaired and a fraction of the catalysts farther away from the solution boundary may remain unused or underused [59,60], which results in lower apparent activities and higher Tafel slopes for ORR at high overvoltages [60–62]. In spite of the potential inaccuracies resulting from large catalyst layer thickness, we decided to conduct all our experiments using a single carbon support loading of 0.4 mg cm^{-2} (0.1 mg total loading), which allowed to fabricate catalyst layers of reasonable quality for all catalysts and Nafion® concentrations. Another reason for selecting such high catalyst loadings was revealed by experiments whose core results are described in Section 3.4.2. Specifically, the experiments performed with intermediate Nafion® quantities, i.e., where the observed kinetic changes were most sensitive to the ionomer content, revealed some loss of Nafion® from the catalyst layers during long experiments. The effects of this undesired phenomenon were virtually eliminated for typical experimental times, when thick catalyst layers were applied. Whenever necessary, the consequences of using such thick catalyst layers will be discussed in the following sections of the paper.

The upper limit of the Nafion® content in the preliminary studies corresponded to R = 1.2. The inks with such Nafion® content did not flocculate over a few weeks (Fig. S1) and created high quality uniform catalyst layers in line with the previously found almost complete surface coverage of the Vulcan surface by the ionomer.

Based on the observed catalyst stabilities under RRDE conditions and the complexity of the respective ORR mechanisms (Supplementary information), only CoPC met the criteria of a model compound to study Nafion® effects on the ORR. The phtahalocyanine catalyzed ORR was found to occur in two waves under RRDE conditions (Fig. 4), whereas a single oxygen reduction wave was observed for the remaining macrocycles. However, the number of electrons transferred in CoPC-catalyzed ORR was independent of the electrode potential and equal ~2 (H_2O_2 reduction product) within the major oxygen reduction wave (Fig. 4), whereas it depended on the electrode potential and Nafion content for the remaining macrocycles (Table S1). In addition, iron macrocycles were easily solubilized at the oxygen reduction potentials (Supplementary information).

We found that ORR was severely inhibited by Nafion® at R = 1.2 for all studied complexes (Fig. 4 and Fig. S2) and that the extent of ORR inhibition correlated with the suppressed double layer currents, which suggested its link to Nafion® adsorption.

3.4. Nafion® effects on the kinetics of ORR catalyzed by CoPC – ionomer and macrocycle loading effects

The still barely acceptable quality of CoPC/Vulcan catalyst layers with R = 0.3 prompted us to increase the lowest Nafion® quantity to R = 0.6 for the kinetic studies. The higher Nafion® content improved the catalyst layer deposition and was still causing no meaningful ORR inhibition.

Inks containing three different CoPC quantities (1.7% (w/w), 5.7% (w/w), and 13.6% (w/w)) and variable quantity of Nafion® (0.6 ≤ R ≤ 2.4) were prepared. The quantities of CoPC in the three inks corresponded to ~100%, 350% and 910% of the full surface coverage, assuming CoPC molecules adsorbed flat on the entire carbon surface [63]. If only basal (graphitic) carbon planes supported the phthalocyanine [64], there would be an excess of the compound for all three catalyst compositions. In either case, all three catalyst compositions were

expected to guarantee the highest possible surface coverage by CoPC molecules with any remaining excess of CoPC forming nonconductive and thus inactive crystals. Indeed, small shiny crystallites of the phthalocyanine were clearly visible under a microscope during the evaporation of the 5.7% and 13.6% inks containing 0.6 μl of 5% Nafion® solution per 1 mg of the carbon support (R = 0.6). While the crystallites were also visible for higher Nafion® contents, their number seemed to decrease with R and virtually none of them could be observed for R ≥ 1.5. Spectrophotometric measurements with CoPC suspensions in mixed IPA + Nafion® solutions revealed that Nafion® had no effect on CoPC solubility in the inks. Therefore, it was reasonable to assume that CoPC crystallites were present in the inks irrespective of the Nafion® content, but their view became progressively obstructed by better dispersed carbon particles in the inks with higher Nafion® concentrations.

3.4.1. CoPC loading effect (R = 0.6)

In agreement with the expected CoPC surface saturation, the activities of the catalysts containing 1.7% and 5.7% CoPC were comparable (Fig. 5). However, the catalyst containing 13.6% CoPC was found more active (Fig. 5). Its higher activity resulted from a higher number of electrochemically active CoPC molecules on the surface as manifested by the better defined CoPC reduction/reoxidation peaks (at ~0.7 V and ~0 V) in the respective voltammograms recorded for that catalyst in oxygen free atmosphere (inset Fig. 5). The faster ORR kinetics was not accompanied by a change in the reaction mechanism, i.e., the number of electrons in ORR stayed virtually identical with that observed for the other two catalysts (see legend of Fig. 5). The higher apparent surface density of the active sites in the 13.6% catalyst may result from a partial overlap between the adsorbed CoPC molecules (i.e., a higher loading than that corresponding to the close packed monolayer) and/or a large number of CoPC crystallites present in the catalyst layer. The latter may act as nonconductive spacers, which reduce the agglomeration of the carbon support particles likely occurring through the strongly hydrophobic phthalocyanine molecules. In consequence, a higher number of the active sites adsorbed on the surface of the carbon support may be exposed and participate in ORR. The results presented in the next section will provide a support for the correctness of the above conclusion.

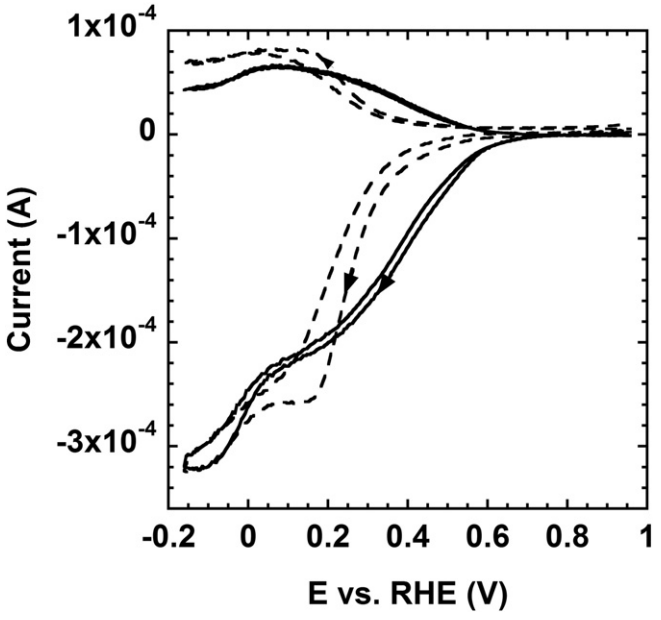

Fig. 4. Background corrected RRDE currents for ORR (disk – negative, ring – positive) recorded for 7.5% CoPC supported on Vulcan XC72 and two Nafion® contents. R = 0.3 - solid lines, R = 1.2 – dashed lines. Total carbon loading 0.1 mg. Rotation rate 400 rpm. Scan rate 10 mV s^{-1}.

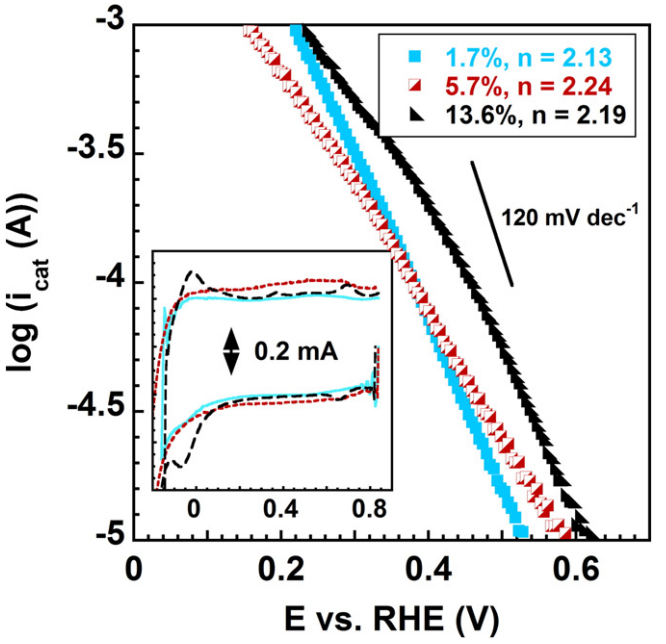

Fig. 5. Kinetic ORR currents determined from first reverse (anodic) scans of RRDE voltammograms measured for various quantities of CoPC supported on Vulcan XC72. R = 0.6. Total carbon loading 0.1 mg. CoPC contents (weight %) listed in the legend. Rotation rate 400 rpm. Scan rate 10 mV s^{-1}. Inset: cyclic voltammograms recorded for the catalysts in absence of oxygen at 100 mV s^{-1}. CoPC contents (weight %): 1.7 – solid blue line; 5.7 – short dashed red line, 13.6 – long dashed black line. Reduction and oxidation peaks corresponding to CoPC are clearly visible only for the 13.6% CoPC (long dashed black line).

The measured Tafel slopes for the three catalysts were ~160 mV dec^{-1} (1.7% CoPC), ~200 mV dec^{-1} (5.7% CoPC) and variable between 160 mV dec^{-1} and 240 mV dec^{-1} (13.6% CoPC). There seems to be no common origin of the differences between the Tafel slopes (Fig. 5). Most likely, the observed differences result from a combination of factors, such as: 1) inaccurate mass transfer correction resulting from the overlap between the two reduction waves (Fig. 4), 2) low and likely potential dependent sample wettability, 3) incomplete catalyst utilization at high overpotentials in the thick catalyst layers [61,62], (especially for the 13.6% catalyst) etc.

3.4.2. Nafion® concentration effects

The Tafel slopes for the vast majority of the studied CoPC catalysts with R > 0.6 were ~180 mV dec^{-1}. In similarity to the results shown in Fig. 5, the Tafel slopes for CoPC catalysts containing various Nafion® quantities were occasionally variable (Fig. S3). Sometimes, an increase of the Tafel slope with overpotential was observed (e.g., Fig. S3 C), suggesting possible catalyst utilization problems in the thick catalyst layers at high overpotentials [59–62,65]. However, the observed changes could not be correlated with any single variable. Consequently, they most likely originated from the overlap between the first and the second reduction wave (Fig. 4) and the resulting inaccuracies of the determination of the limiting current and the mass transfer correction. An underestimated limiting current is expected to produce a decrease of the Tafel slope with overpotential (a concave Tafel plot), whereas an overestimated limiting current would produce a convex Tafel plot (overpotential driven Tafel slope increase). Because of the above problems, we decided to evaluate the kinetic effects of Nafion® at low overpotentials, where the possible errors resulting from inaccurate mass transfer correction as well as incomplete catalyst utilization are lowest.

Fig. 6 demonstrates the effects of increasing quantity of Nafion® on the catalytic activity for ORR of the catalysts containing 1.7%, 5.7% and 13.6% CoPC. The reaction on all catalysts becomes strongly inhibited,

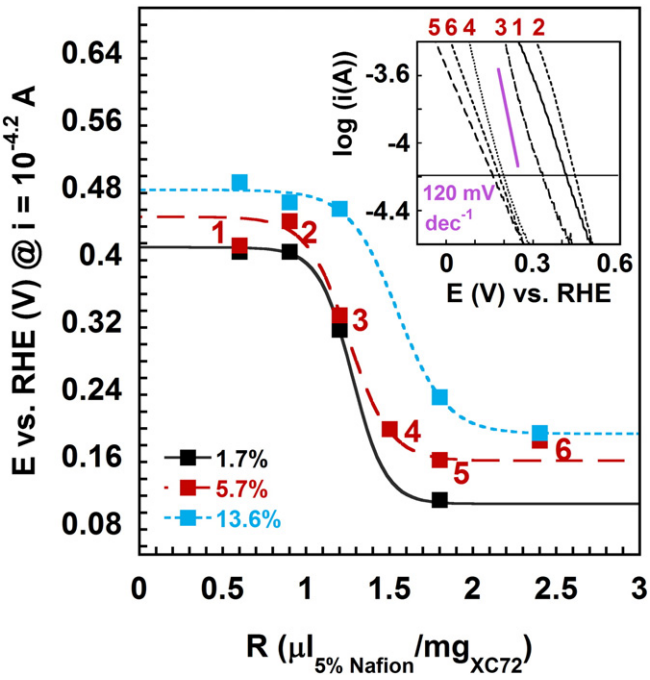

Fig. 6. Oxygen reduction potential corresponding to a constant geometric current density of 6.3×10^{-5} A cm^{-2} plotted against the Nafion® content (R) in the ink for three XC72 supported catalyst containing 1.7%, 5.7% and 13.6% CoPC. Inset: Tafel plots for the 5.7% catalyst also showing a Tafel slope of 120 mV dec^{-1} (purple line). The average number of electrons transferred in ORR for different R (n(R)): 1.7% CoPC – 2.13 (0.6), 2.11 (0.9), 2.16 (1.2), 2.11 (0.8); 5.7% CoPC – 2.24 (0.6), 2.16 (0.9), 2.14 (1.2), 2.16 (1.5), 2.32 (1.8), 2.13 (2.4); 13.6% CoPC – 2.19 (0.6), 2.07 (0.9), 2.26 (1.2), 2.12 (1.5).

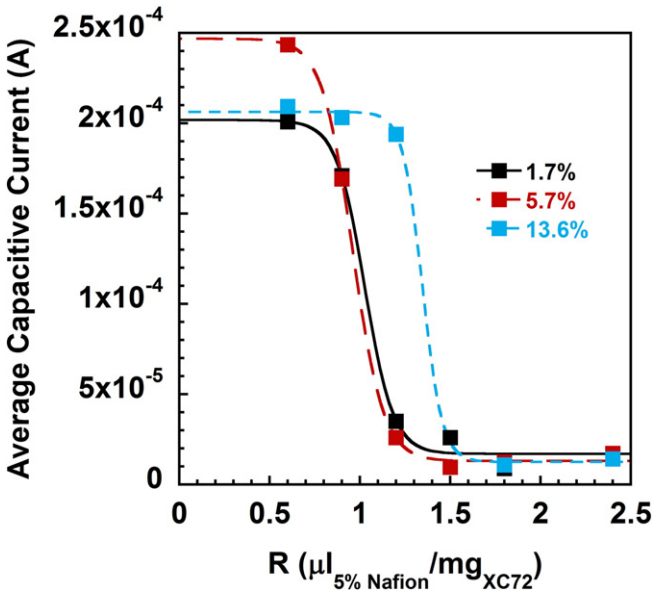

Fig. 7. Capacitive currents at 0.3 V for three CoPC + XC72 catalysts plotted against the Nafion® content (R) in the ink. The values plotted are average currents measured in both forward and reverse voltammetric scans recorded at a scan rate of 100 mV s^{-1} at 0.4 V vs. RHE. Total Vulcan XC72 loading 0.1 mg.

when Nafion® concentration in the catalyst increases. The observed reduction potentials shift cathodically by as much as 300 mV, when the Nafion® content increases from R = 0.6 to R = 1.8. The changes in ORR kinetics for all three catalysts do not have a continuous character but occur stepwise within a narrow concentration range of Nafion®. The kinetic changes are not accompanied by meaningful changes in the reaction selectivity for hydrogen peroxide (number of electrons in ORR listed in the figure caption). The catalysts containing 1.7% and 5.7% CoPC behave similarly in that a change in the reaction kinetics is already advanced at R = 1.2. For the catalyst containing 13.6% CoPC, the major kinetic change occurs after R reached 1.2. A similar "delay" is also visible in the graph showing the suppression of the respective capacitive currents, which indicates that the origin of the inhibition is Nafion® adsorption (Fig. 7).

The "delay" may have its origin in the already postulated effect of CoPC crystallites acting as carbon particle separators, which can make a larger fraction of the carbon surface accessible but can also compete with the carbon particles as the hydrophobic centers for the self-assembly of Nafion®.

Most importantly, the ORR inhibition for all catalyst compositions closely correlates with the Nafion® adsorption, whose presence is reflected in the respective capacitive currents (Fig. 7), and with the ink dispersion behavior shown in Fig. S1.

3.5. The effect of Nafion® on ORR catalyzed by carbon supported platinum

For consistency with the data obtained for CoPC, the measurements for the Pt catalysts were also performed for the total carbon loading of 0.1 mg (0.4 mg cm^{-2}). In spite of the identical Pt content (4.8%) in the two low Pt loading catalysts, there were measurable differences in their electrochemistry. The Pt4.8G catalyst (Fig. 8) exhibited generally lower background currents than the catalyst supported on Vulcan (Pt4.8V) in the whole studied potential range, i.e., in the hydrogen UPD (H_{UPD}), PtO formation/reduction and the double layer (determined predominantly by the carbon support) regions. This was true for all Nafion® concentrations in the inks.

The lower double layer currents for Pt4.8G have the origin in the more graphitic character (see Fig. 3) of its carbon support and its lower specific surface area (156 m^2 g^{-1} for the catalyst) compared to that of Vulcan in Pt4.8V (~240 m^2 g^{-1}). Likewise, lower H_{UPD} and Pt oxide currents measured for Pt4.8G are expected from its larger Pt particle size (4.8 nm) compared to that of Pt4.8V (number averaged 2.2 nm, surface averaged 2.6 nm [43]).

Both low Pt loading catalysts were affected by increased Nafion® concentration (R) in a way qualitatively similar (Fig. 8) to that observed for the organic macrocycles. The background currents in the whole potential range dropped virtually stepwise with an increase in the Nafion® content in the ink demonstrating that both carbon and Pt surfaces were blocked by the ionomer. The currents measured for the Pt20V in deoxygenated solutions were significantly less affected by Nafion® than those for Pt4.8V and Pt4.8G. The double layer currents were completely insensitive to the Nafion® content up to R = 2.5. The increase in Nafion® content caused small changes in the shape of hydrogen underpotential deposition (H_{UPD}) peaks, but the changes were associated with no meaningful decrease in the electrochemical surface area (ECSA) determined from H_{UPD}. The comparison of ECSA for all studied catalysts is shown in Fig. 9.

Well defined correlations were also observed between the ECSA and the suppression of the double layer currents (Fig. 10) for the two low Pt content Pt (Pt4.8V and Pt4.8G), which indicated a link between the Pt surface area loss and Nafion® adsorption on the carbon support. It is seen from Fig. 9 that a major drop in the measured ECSA for the Pt4.8V catalyst occurred before R reached 1.5, i.e., in the very similar concentration range to that causing the self-assembly of Nafion® on both Vulcan and CoPC/Vulcan. The finding suggests that the surface of the carbon support is the major factor determining the self-assembly of Nafion® not only on CoPC/Vulcan but also on Vulcan supported 4.8% Pt (Pt4.8V).

The effects of Nafion® on the electrochemistry of Pt4.8G in deoxygenated solutions were quantitatively similar to those observed for Pt4.8V, i.e., occurred in the similar Nafion® concentration range (Fig.

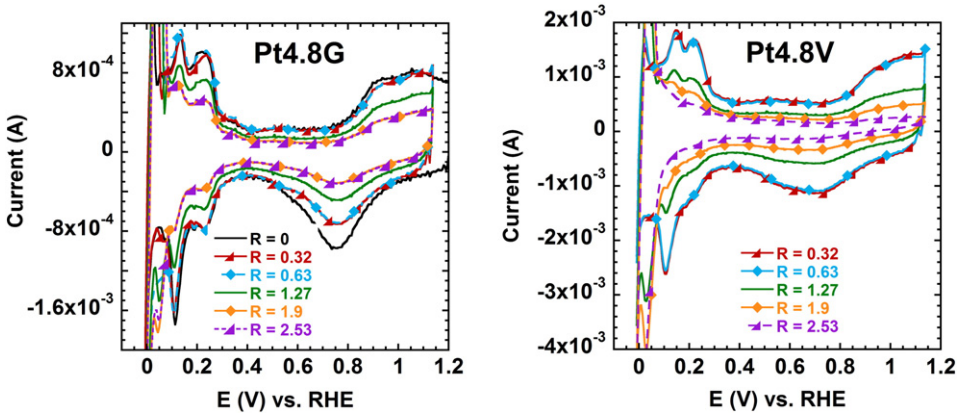

Fig. 8. Background currents measured for Pt4.8G and Pt4.8V catalysts containing various quantities (R) of Nafion®. Scan rate 200 mV s^{-1}. Total carbon support loading 0.1 mg.

9) in spite of the lower specific surface area of that catalyst (157 m^2 g^{-1}). This finding does not contradict the fact that Nafion® self-assembly is promoted by graphitic surfaces, as demonstrated previously in this paper and elsewhere [53,54]. The Nafion® induced changes in the double layer charging currents (Fig. 8) are proportional to the sum of contributions of the very different double layer capacities of uncoated and Nafion® coated graphitic and non-graphitic carbon surfaces (Fig. 3). In addition, before the maximum surface coverage is reached, the relative extent of blocking of graphitic and non-graphitic surfaces may change with the overall surface coverage. This may lead to a departure from the direct proportionality between the measured double layer capacity and the actual total surface occupied by the self-assembled ionomer (Eq. 1). Such effects, in addition to the differences in Pt particle size (4.8 nm for Pt4.8G and 2.2 nm for Pt4.8V [43]) also contribute to the observed changes in ECSA.

In Fig. 11 are shown the ORR Tafel plots for the two low Pt content catalysts. The variable slopes of the plots recorded for the catalyst layers containing lower Nafion concentrations (R ≤ 1.27) most likely result from the large thickness of the catalyst layers and/or non-uniform catalyst distribution on the disk [58], whose extent may be affected by the Nafion® content. The ECSA in those layers has not yet dropped to its low level (Fig. 9) and the effects of incomplete catalyst utilization at high overpotentials are visible as increases in the apparent Tafel slopes.

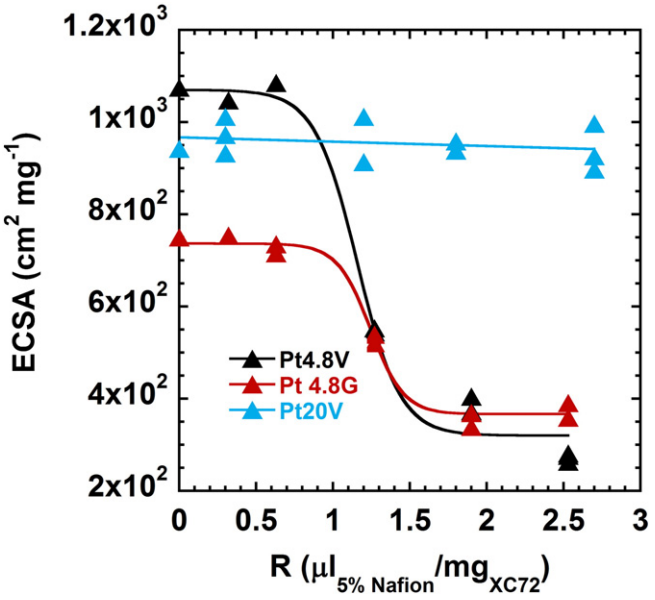

Fig. 9. Electrochemical surface area for Pt catalysts determined from H_{UPD} at 100 mV s^{-1} plotted vs. Nafion® content in the catalyst layer.

The Tafel slopes for the less active catalyst layers (R > 1.27) are virtually constant, which corroborates with their lower volumetric activity, as expected from other theoretical [61,62] and experimental [56,59,60] work. However, the catalyst layer thickness effects do not take precedence over Nafion® induced kinetic effects. As expected from the observed changes in ECSA (Figs. 9 and 10), the ORR currents measured for both 4.8% Pt catalysts (Fig. 11) become visibly suppressed in presence of larger Nafion® quantities and the extent of ORR inhibition occurs rather stepwise within a narrow range of Nafion® concentrations. The oxygen reduction potentials are shifted by up to 60 mV, which corresponds to a ~3-fold decrease in the kinetic current, in agreement with the observed losses in ECSA (Figs. 9 and 10).

The kinetic changes were not accompanied by any appreciable change in the virtually 100% reaction selectivity for water formation (4-electron ORR) versus the hydrogen peroxide formation (2-electron ORR). The largest negative departure from 4 of the number of electrons (n) involved in ORR was only 0.05 for the Pt4.8V catalyst at R = 1.90 (n = 3.95). The highest H_2O_2 generation (Pt4.8V at R = 1.90) observed by us in H_2SO_4 is lower than that reported for Nafion® coated polycrystalline Pt electrode in less adsorbing $HClO_4$ solutions by Ohma and coworkers [57]. The most likely reason for this apparent discrepancy is the large thickness of our catalyst layers. Hydrogen peroxide generated

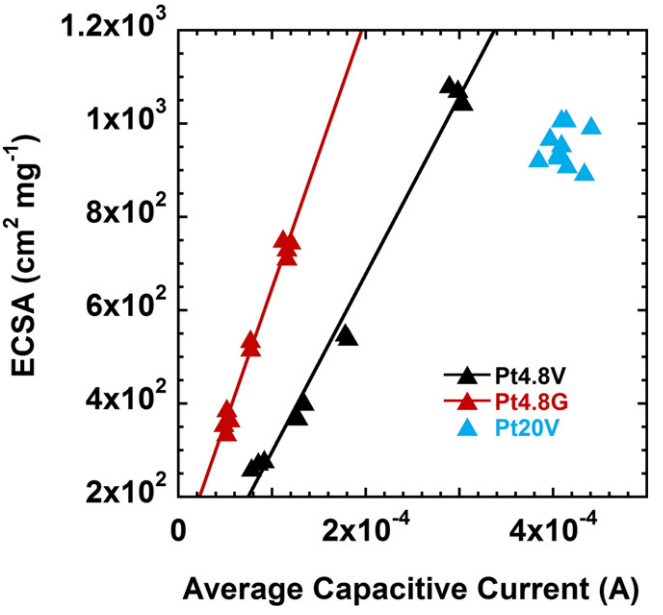

Fig. 10. Electrochemical surface area for Pt catalysts determined from H_{UPD} plotted vs. average (cathodic and anodic) double layer current at 0.35 V vs. RHE. Data obtained at a scan rate of 100 mV s^{-1}.

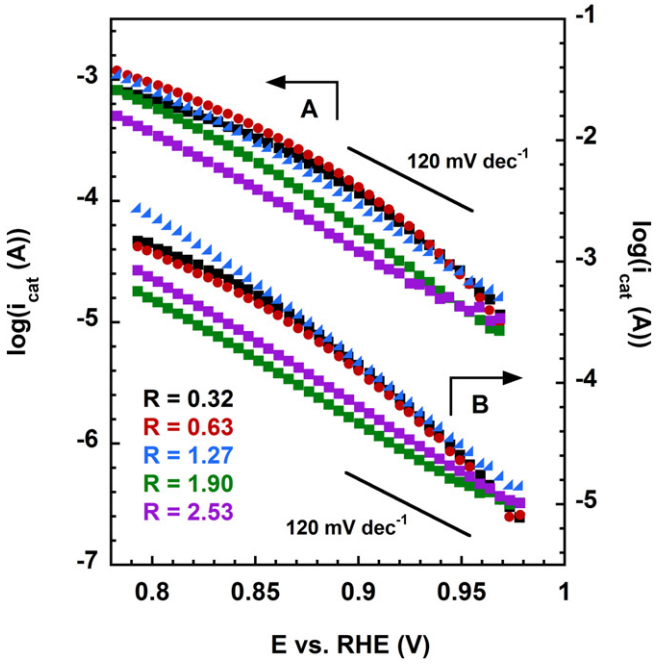

Fig. 11. ORR kinetic currents measured for Pt4.8G (A) and Pt4.8V (B) catalysts containing various quantities (R) of Nafion®. Scan rate 10 mV s^{-1}. Rotation rate 400 rpm. Scan directions indicated by the arrows parallel to the Tafel plots.

deep inside a catalyst layer has to travel to the layer/solution boundary in order to be detected on the ring of an RRDE. The thicker the layer, the larger the chances that peroxide will undergo subsequent reduction to water and will not be detected as the ORR product. However, even if substantially thinner catalyst layers were applied, the ORR would not change from a predominantly four- to a predominantly two-electron process as a result of Nafion® adsorption. This is because Nafion® does not block individual Pt atoms but continuous fractions of the Pt surface area [66] still leaving the remaining continuous fractions untouched and available for ORR.

In line with the above reasoning about Nafion® morphology in the vicinity of carbon supported Pt particles, the extent of surface blocking and the magnitude of the kinetic effects were smaller for Pt4.8V and Pt4.8G than those observed for CoPC and other macrocyclic catalysts. The latter are active only as isolated or at most partially overlapping molecules, which can be easily excluded from the reaction if blocked by the ionomer.

Some differences were observed between the ORR kinetics (Fig. 11) for the two low Pt content catalysts. For Pt4.8G, the kinetic ORR currents were lowest for the ink containing the highest Nafion® quantity (R = 2.53), whereas the slowest ORR kinetics for the Pt4.8V was observed at R = 1.9. The kinetic behavior of Pt4.8V at R = 2.53 does not correlate with the measured loss in ESCA (Fig. 9). The likely reason for that discrepancy were differences in the catalyst distribution on the disk surface, which are known to lead to similar effects in drop coated catalyst layers [58]. The discrepancy between the kinetic and the ECSA data may also have its origins in different scan rates employed in the respective determinations. A scan rate of 100 mV s^{-1} was used in the ECSA, whereas a 10 mV s^{-1} scan rate was applied in the kinetic studies. Slow scan rates may enable a potential/Pt surface driven restructuring [67] and possibly also promote Nafion® desorption and formation of small ionomer aggregates. The lack of a similar effect for Pt4.8G may be associated with the stronger interaction of its more graphitic surface with the hydrophobic Nafion® backbone.

It has to be mentioned that no ECSA and ORR kinetic losses were observed for Pt4.8G and Pt4.8V when a 1:100 diluted Nafion® solution was deposited on top of their Nafion® free layers in quantities corresponding to R as high as 5. The finding confirms that the carbon surface blocking by Nafion® emerges as a result of (directional) molecular interactions between the surface and the ionomer rather than from a statistically preferred contact with the hydrophobic backbone of the ionomer.

In agreement with the lack of Nafion® effect on the ECSA of Pt20V up to R = 2.7 (Fig. 9), the RRDE voltammograms recorded for the catalyst in oxygenated solutions were not substantially affected by Nafion® within that range of concentrations. The same was true for the number of electrons transferred in ORR, which did not deviate from 4 by >0.02 under all studied conditions. In Fig. 12 are shown the respective Tafel plots for Pt20V. The measured ORR kinetics, while somewhat affected by the large thickness of the catalyst layers (Tafel plot curvature), remains almost unaffected by Nafion® concentration, which in effect indicates the lack of Pt surface blocking by the hydrophobic backbone of the ionomer. Slightly slower ORR kinetics visible for the catalyst ink with R = 1.8 in Fig. 12 likely have its origins in.

small morphological differences of the catalyst layers containing different but small (not exceeding 13% of the total volume) quantities of Nafion®, which likely forms some bulk phase in absence of the self-assembly phenomenon. The lack of the phenomenon in Pt20V layers containing up to R = 2.7 of the ionomer results from the catalyst's significantly higher ratio of the Pt to carbon surface areas compared to the low Pt content catalysts. For Pt20V, the ratio is ~5 times higher than for Pt4.8V and ~5.6 times higher than for Pt4.8G based upon the measured ECSAs (Fig. 9) and the BET surface areas. While hydrophobic carbon surfaces in all Pt catalysts promote the self-assembly, more numerous hydrophilic Pt particles in Pt20V disrupt it. The interference may be both passive (steric effects) and active (adsorption of the hydrophilic sulfonic groups on the Pt surface).

The lack of Nafion® self-assembly on Pt20V up to R = 2.7 does not contradict the results by Ma Andersen [40] who observed Nafion® adsorption on a 20% Pt/Vulcan catalyst with the maximum surface coverage of 8.58×10^{-2} g/g, i.e., corresponding to our R ≈ 2.3 after the correction for the Pt content. In particular, it does not exclude Langmuirian adsorption of Nafion® on Pt20V from solution. In fact, the adsorption of Nafion® on a 20% Pt/Vulcan catalyst was shown to be significantly weaker (equilibrium constant 8.88) than that on pure Vulcan (equilibrium constant 18.19) [40], which remains in agreement with the above postulated disrupting effect of Pt particles on the self-assembly.

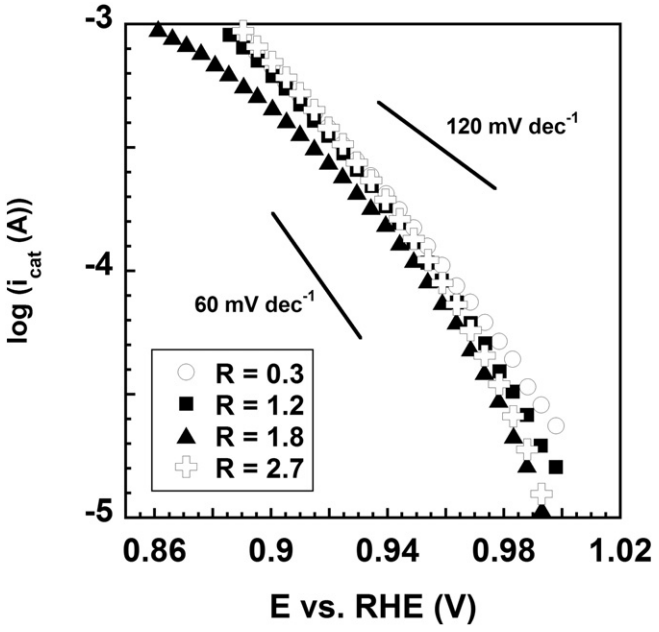

Fig. 12. ORR kinetic currents measured for Pt20V (0.1 mg total carbon loading) containing various Nafion® quantities (R). Scan rate 10 mV s^{-1}. Rotation rate 400 rpm.

While the self-assembly of Nafion® is predominantly governed by major attractive forces involving the ionomer's backbone and the carbon support surface, the magnitude of the ORR kinetic effects may also depend on the liquid electrolyte. For instance, a larger Nafion® induced decrease in the apparent ORR kinetics may be expected for carbon supported Pt catalysts in less adsorbing $HClO_4$ electrolytes than in the present case. The side chains of self-assembled Nafion® likely exhibit a sufficient degree of mobility to allow at least some of the sulfonic groups adsorb on neighboring Pt particles and lower their apparent activity in ORR. In consequence, the ORR kinetics in $HClO_4$ would be lowered by self-assembled Nafion® as a result of both the ionomer's hydrophobic backbone spillover onto the Pt surface and the sulfonic group adsorption. On the other hand, no significant effect from the sulfonic group adsorption can be expected in presence of a large excess of HSO_4^- ions strongly competing for the Pt adsorption sites in sulfuric acid solutions.

3.6. Koutecky-Levich analysis of the limiting currents

Oxygen diffusing inside thick catalyst layers such as those used in the present study, may be unable to reach the catalyst particles deep inside such layers during a typical RDE experiment. The problem frequently results from the inherently slow oxygen diffusion in the tortuous channels of the layer, the competition between the active sites closer and farther away from the catalyst layer/solution boundary or both. The high electrical resistance in the narrow channels may also contribute to the problem. Irrespective of its origin, significant oxygen transport impairment within a catalyst layer can create the conditions mimicking a loss of the catalytic activity [59,62,65,68,69]. The small Nafion® quantities in the studied catalyst layers were not expected to significantly affect the existing or create additional barriers for oxygen transport inside the thick catalyst layers studied by us. However, in extreme cases [59], oxygen transport within thick catalyst layers can be so slow and the active sites not sufficiently abundant that a limiting current potentially sustainable through oxygen diffusion in solution cannot be maintained by the reduction of oxygen diffusing through a thick catalyst layer. In such cases, the limiting current measured with an RDE or RRDE is lower than that expected from the convective diffusion of oxygen in solution. On the other hand, the ORR limiting current may be lowered even in absence of any transport limitations inside the catalyst layer, e.g., when a thick ionomer layer is deposited on top of the catalyst layer and oxygen diffusion through the ionomer film is slow. Such phenomena are easily detected and quantified when inverse limiting currents are plotted vs. the inverse electrode rotation rate (Koutecky-Levich [70] plots) without the need to know a priori the solution viscosity, the number of electrons transferred in ORR or the oxygen diffusion coefficient. On the other hand, they can be easily overlooked if, as in the present study, the standard mass transfer correction is used, as the latter assumes that the oxygen diffusion in solution determines the limiting current.

The Nafion® induced exclusion of ~99% of the active sites in the CoPC catalyst layers could potentially create a situation, where the active site density were so small that the limiting ORR current would be suppressed. Also, if for any unexpected reason, the ionomer migrated from within the catalyst layer to its outermost surface, it could create a transport limitation that would be overlooked if only the standard mass transfer correction was applied to determine the kinetic parameters of the reaction.

In Fig. 13 are shown the intercepts of Koutecky-Levich [70] plots obtained for the limiting oxygen reduction currents recorded for the two low Pt loading catalysts (Pt4.8V and Pt4.8G) and a 4.2% CoPC adsorbed on Vulcan XC72. Within an experimental error, the intercepts obtained for the Pt catalysts are equal zero for all Nafion® contents. Due to the overlap between the first and the second ORR wave for CoPC (Fig. 4), the respective intercepts determined for the first two-electron reduction wave are disturbed by much larger errors. However, they still

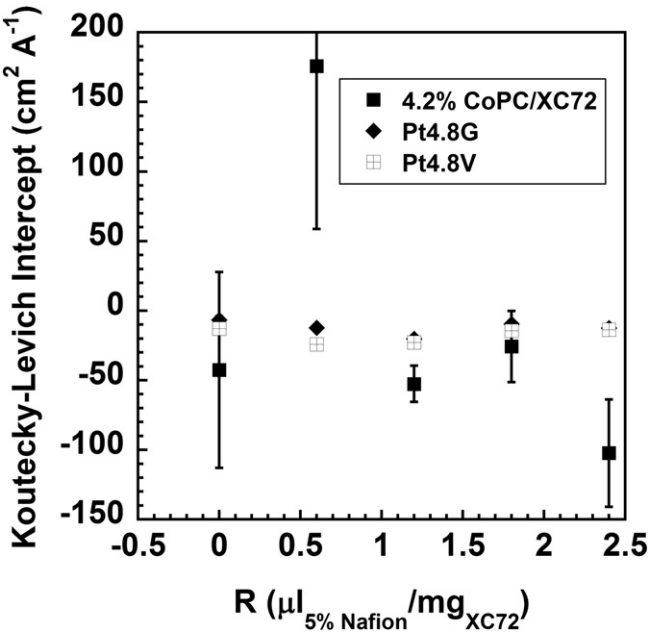

Fig. 13. Intercepts of the Koutecky-Levich plots for the limiting ORR currents in O_2 saturated solutions measured from experiments performed at 400, 625, 900, 1225, 1600, 2025 and 2500 rpm rotation rates. The error bars reflect the respective errors of the intercepts obtained from the linear fitting and are too short to be seen for the Pt catalysts.

oscillate around zero and do not exhibit any meaningful trend. These results demonstrate that the kinetic data obtained using the standard mass transfer corrections were affected by none of the above phenomena. They also indicate that the major kinetic effects of small Nafion® additions observed by us cannot be attributed to any dramatic changes in the catalyst layer morphology. As already postulated, the active sites are simply blocked by the hydrophobic component of the self-assembled ionomer.

Steric barriers and the overall Pt surface hydrophilicity in aqueous media do not allow for complete blocking of all facets of nanocrystalline Pt, which results in the relatively weaker ORR inhibition. The flatly adsorbed molecular catalysts (CoPC and other macrocycles studied) do not create meaningful steric barriers. To the contrary, their hydrophobic character promotes attractive interactions with the hydrophobic Nafion® component. Consequently, the only macrocyclic catalytic centers that remain active in the presence of self-assembled Nafion® must be adsorbed in one of the two favorable locations. These are either below small imperfections (openings) in the self-assembled layers or located in such parts of the carbon surface that were excluded from the self-assembly. Disorganized (non-graphitic) and partially oxidized surfaces can be more likely excluded from Nafion® self-assembly due to their increased hydrophilicity. Other parts may be unaffected by the self-assembly because of a mismatch between their overall size (surface area) and the length of the adsorbed Nafion® strand(s).

4. Discussion

The results presented in the previous sections demonstrate a significant affinity of Nafion® to pure Vulcan XC72, all non-precious macrocyclic complexes adsorbed on XC72 and low Pt content (4.8%) carbon supported catalysts but not to 20% Pt/Vulcan XC72. These observations demonstrate that the self-assembly of Nafion® on the catalysts is predominantly determined by graphitic surfaces of the carbon support, but it is also influenced by the number, size and surface properties of the catalyst particles. The self-assembled layers of Nafion® led to a decrease of the kinetic ORR currents on the transition metal catalysts by up to two orders of magnitude, whereas the kinetics of ORR on the two low Pt loading (4.8%) catalysts decreased under similar conditions

by less than one order of magnitude (Fig. 9). The differences in ORR inhibition between the Pt catalysts and the macrocyclic catalysts reflect the differences in their morphology. Phthalocyanines and porphyrins in a crystalline form cannot participate in electrocatalysis, as they are non-conductive. The non-crystalline macrocyclic complexes can participate in ORR catalysis only if the 3d orbitals of their central atoms simultaneously and effectively overlap with the surface orbitals of the carbon support and the acceptor orbitals in oxygen molecule. This is possible only for flatly adsorbed and isolated or at most partially overlapping molecules. Such an orientation is virtually universal for phthalocyanines, porphyrins and corroles adsorbed on a vast variety of substrates including metallic [71–74], semi-conducting [75], and non-conductive [76] materials, but most of all on graphitic surfaces [77–82], where strong attractive dispersion interactions exist between the delocalized π-electron clouds of the adsorbates and the surface. Due to the flat orientation of the (hydrophobic) adsorbed catalytic molecules on the hydrophobic surface, neither the surface hydrophobicity nor its morphology is significantly affected by the adsorption. In consequence, the hydrophobic component of Nafion® can easily adsorb on both bare and catalyst coated carbon surfaces. The adsorbed macrocyclic complexes can participate in ORR only when they are not completely blocked by the hydrophobic backbone of Nafion®. In order for this to happen, they must be located either below small openings between the adsorbed ionomer chains on the predominantly graphitic surfaces or in such locations, where the local surface morphology or, less likely [64], more hydrophilic surface character, prevented Nafion® adsorption. Obviously, only a very small fraction of the catalytically active molecules fulfills either condition in presence of self-assembled Nafion®. The approximately two order of magnitude decrease in ORR kinetics resulting from the Nafion® self-assembly on the CoPC catalysts (Fig. 8) demonstrates that only 1% of the active centers retain their ability to reduce oxygen under such conditions.

The situation is significantly different for the Pt catalysts. The preferred orientation of Nafion® molecules in contact with an oxidized Pt is that with its hydrophilic component facing the hydrophilic oxidized surface. In presence of liquid water (electrolyte), Nafion® maintains an open morphology [36] at its interface with bare Pt surfaces, even if its hydrophobic component previously occupied that interface in absence of liquid water [67]. Moreover, as oxygen was not eliminated during the preparation of the Pt catalyst inks, the surface of Pt particles was at last partially oxidized and thus strongly hydrophilic. Therefore, no Pt surface blocking is expected for carbon supported Pt catalysts under RRDE conditions unless the hydrophobic interactions between the catalyst support and Nafion® backbone are strong enough to impose the same Nafion® orientation over the neighboring Pt particles. Such an effect does not occur for Pt20V up to R = 2.7, but it already reaches saturation at R = 2.5 for the two low Pt loading catalysts. One can expect that both the overall (hydrophilic) Pt surface area compared to that of (hydrophobic) carbon and the distribution of Pt particles on the carbon surface determine the extent of the Nafion® effects. In this regard, the differences between the high (Pt20V) and the low (Pt4.8 V) Pt loading catalysts can be correlated with both the larger relative Pt surface area in Pt20V and the shorter average distances between its Pt particles than those in Pt4.8V. Assuming an ideal hexagonal Pt particle distribution in both cases, one can demonstrate that the average distance between ~2.1 nm [45] Pt nanocrystals supported by ~30 nm [44] Vulcan particles in Pt20V is ~9 nm, but it approaches ~22 nm between similar ~2.2 nm Pt particles in Pt4.8V [43].

The only slightly stronger inhibiting effect of Nafion® on ORR catalyzed by Pt4.8G than that observed for Pt4.8V cannot be easily explained, as it results from the combination of a number of factors whose relative importance remains unknown. The larger size of Pt particles in Pt4.8G (4.8 nm) compared to that in Pt4.8V (2.2 nm) results in their ~4.8 smaller (hydrophilic) surface area and ~10 times smaller number. In addition, the particles in Pt4.8G are deposited on more hydrophobic graphitized carbon. As will be demonstrated in a forthcoming paper, the absolute carbon surface area and consequently the fraction of the total carbon surface area affected by the self-assembly is larger in Pt4.8G. All these factors should lead to a less disrupted self-assembly of Nafion® on Pt4.8G and likely to a more significant ORR inhibition. However, steric barriers can potentially make the larger Pt nanocrystals in Pt4.8G more difficult to block. In addition, the actual and unknown Pt particle distribution [83] is also expected to affect the observed phenomena.

Detrimental effects of Nafion® on the accessible surface area and activity of carbon supported Pt catalysts have been known [3–7,59]. What differentiates the results of the present work is that they were obtained for very low Nafion® contents in the catalyst layer. The highest Nafion® concentration used in the present work was ~10% (R = 2.5), whereas the major changes observed for the two low Pt content catalysts were already complete between 6% and 8% of Nafion® in the catalyst layer (1.5 ≤ R ≤ 2.0). As already demonstrated, such low quantities were sufficient to create just a single monolayer of Nafion® on the studied carbon supports, but no bulk ionomer phase.

A continuous network of ionically conducting (bulk) Nafion® clusters intermingled with gas channels is necessary to provide the required proton conductivity and oxygen access in fuel cell catalyst layers. Most likely for that reason, Nafion® effects on the performance of carbon supported Pt catalysts are typically studied for ≥20% contents of the ionomer. The question whether there is a link between the inhibition phenomena observed in this work and, for instance the work by Guilminot et al. [59], where 50% Nafion® concentration was used, is not easy to answer. Self-assembly of Nafion® would not occur if there was no driving force for it. Our results demonstrate that the self-assembly does not disappear and so does not the driving force, when Nafion® concentration increases slightly above that required to form a monolayer (6%–8%). However, they cannot be extrapolated to significantly higher Nafion® concentrations (50%), where a bulk ionomer phase is undoubtedly present in large quantities. No monolayer but ~7 nm Nafion® clusters were observed by electron tomography [50] in Vulcan/Nafion® layers containing 17% and 33% of the ionomer, but the layers used in Ref. [50] were hot-pressed before the tomography. Hot-pressing is commonly applied to fuel cell catalyst layers, as it helps to distribute (bulk) polymer electrolyte and create at the same time a desired pore structure [68,84] for oxygen transport. As our samples were not heat treated, the present data cannot be extrapolated to fuel cell conditions, either. However, one cannot exclude some effect of the thermodynamic forces responsible for Nafion® self-assembly on the final morphology of Pt/C/Nafion® fuel cell catalyst layers.

The present study does not allow for quantitative estimates of the magnitude of potential adverse effects of Nafion® on the measured activities of novel ORR catalysts in aqueous media. However, its conclusions regarding the roles of the catalyst and catalyst support particle hydrophobicities/hydrophilities, their relative surface areas, sizes, etc., may be helpful in preliminary assessments of such effects. For instance, especially strong adverse Nafion® effects are expected for the catalysts utilizing highly hydrophobic supports, e.g., unmodified carbon nanotubes or the catalysts whose active centers are embedded in hydrophobic surfaces. Among the latter are heat treated and related ORR catalysts [11–13], which are structurally similar to the transition metal macrocycles studied by us, i.e., their active centers are embedded in π - electron rich environments.

Most importantly, the self-assembly of Nafion® around carbon supported catalyst particles and the formation of micelle-like structures with hydrophobic core and hydrophilic shell has critical consequences for the catalyst activity determinations using rotating disk electrodes. The phenomenon is deceiving in that it helps making high quality, well dispersed inks, which meet the criteria for accurate RRDE measurements [23]. However, it also leads to ORR inhibition and underestimated catalyst activities. The probability of erroneous catalyst activity determination is increased by the fact that the presence of Nafion® self-assembly can likely remain unnoticed. Firstly, it does not manifest itself in

Koutecky-Levich analysis. Secondly, its occurrence is triggered by minute changes in the Nafion® concentration in catalyst inks, which may be inadvertently introduced, e.g., when using older and partially evaporated ionomer solutions. It is not our intention to arbitrarily pick some published work and critically review it from the perspective of possible Nafion® effects on the reported data. In this regard, it should be sufficient to admit that our own results obtained for FeTPP were also affected by the phenomenon and the magnitude of the effect of the axial coordination of the active center by polyvinylimidazole on ORR was overestimated [85].

5. Conclusions

- Nafion® tends to self-assemble through its hydrophobic backbone on high surface area carbon blacks typically used as supports for fuel cell oxygen reduction catalysts.
- Nafion® self-assembly is mostly promoted by hydrophobic graphitic surfaces, but can also be imposed over neighboring non-graphitic or non-hydrophobic surfaces (self-assembly spillover).
- Spillover of self-assembled Nafion® onto catalytically active sites in carbon supported oxygen reduction catalysts impairs the catalyst activity.
- The extent of active site blocking is determined by surface hydrophobicity/hydrophilicity in the immediate vicinity of the active sites and by steric/geometric factors. Adsorbed hydrophobic molecules, e.g., phthalocyanines and isolated sites embedded in hydrophobic surfaces can be almost completely deactivated, whereas only a fraction of the surface area of hydrophilic Pt nanocrystals can be blocked.
- The use of Nafion® as an ink dispersing agent for catalyst activity testing in aqueous electrolytes creates a serious risk of significant underestimating the catalyst activity.

Acknowledgement

The authors want to express their gratitude for the financial support from the UC Office of the President (Lab Fees Research Program, grant ID# 12-LR-237440).

Appendix A. Supplementary data

Supplementary data to this article can be found online at http://dx.doi.org/10.1016/j.jelechem.2016.09.014.

References

[1] K.A. Mauritz, R.B. Moore, State of understanding of Nafion, Chem. Rev. 104 (2004) 4535–4585.
[2] Z.D. Wei, H.B. Ran, X.A. Liu, Y. Liu, C.X. Sun, S.H. Chan, P.K. Shen, Numerical analysis of Pt utilization in PEMFC catalyst layer using random cluster model, Electrochim. Acta 51 (2006) 3091–3096.
[3] G. Sasikumar, J.W. Ihm, H. Ryu, Dependence of optimum Nafion content in catalyst layer on platinum loading, J. Power Sources 132 (2004) 11–17.
[4] N. Wagner, T. Kaz, K.A. Friedrich, Investigation of electrode composition of polymer fuel cells by electrochemical impedance spectroscopy, Electrochim. Acta 53 (2008) 7475–7482.
[5] M. Lee, M. Uchida, H. Yano, D.A. Tryk, H. Uchida, M. Watanabe, New evaluation method for the effectiveness of platinum/carbon electrocatalysts under operating conditions, Electrochim. Acta 55 (2010) 8504–8512.
[6] O.J. Curnick, B.G. Pollet, P.M. Mendes, Nafion1-stabilised Pt/C electrocatalysts with efficient catalyst layer ionomer distribution for proton exchange membrane fuel cells, RSC Adv. 2 (2012) 8368–8374.
[7] A. Ignaszak, S. Ye, E. Gyenge, A study of the catalytic Interface for O2 electroreduction on Pt: the interaction between carbon support meso/microstructure and ionomer (Nafion) distribution, J. Phys. Chem. C 113 (2009) 298–307.
[8] H. Gharibi, F. Yasi, M. Kazemeini, A. Heydari, F. Golmohammadi, Fabrication of MEA based on sulfonic acid functionalized carbon supported platinum nanoparticles for oxygen reduction reaction in PEMFCs, RSC Adv. 5 (2015) 85775–85784.
[9] A. Ohma, T. Mashio, K. Sato, H. Iden, Y. Ono, K. Sakai, K. Akizuki, S. Takaichi, K. Shinohara, Analysis of proton exchange membrane fuel cell catalyst layers for reduction of platinum loading at Nissan, Electrochim. Acta 56 (2011) 10832–10841.
[10] J.P. Owejan, J.E. Owejan, W. Gu, Impact of platinum loading and catalyst layer structure on PEMFC performance, J. Electrochem. Soc. 160 (8) (2013) F824–F833.
[11] B. Wang, Recent development of non-platinum catalysts for oxygen reduction reaction, J. Power Sources 152 (2005) 1–15.
[12] R. Othman, A.L. Dicks, Z. Zhu, Non precious metal catalysts for the PEM fuel cell cathode, Int. J. Hydrog. Energy 37 (2012) 357–372.
[13] Z. Chen, D. Higgins, A. Yu, L. Zhang, J. Zhang, A review on non-precious metal electrocatalysts for PEM fuel cells, Energy Environ. Sci. 4 (9) (2011) 3167–3192.
[14] A. Morozan, S. Campidelli, A. Filoramo, B. Jousselme, S. Palacin, Catalytic activity of cobalt and iron phthalocyanines or porphyrins supported on different carbon nanotubes towards oxygen reduction reaction, Carbon 49 (2011) 4839–4847.
[15] S. Fukuzumi, Y. Yamada, K.D. Karlin, Hydrogen peroxide as a sustainable energy carrier: electrocatalytic production of hydrogen peroxide and the fuel cell, Electrochim. Acta 82 (2012) 493–511.
[16] J.-M. Saveant, Molecular catalysis of electrochemical reactions. Mechanistic aspects, Chem. Rev. 108 (2008) 2348–2378.
[17] J.H. Zagal, Metallophthalocyanines as catalysts in electrochemical reactions, Coord. Chem. Rev. 119 (1992) 89–136.
[18] J. Rosenthal, D.G. Nocera, Role of proton-coupled electron transfer in O–O bond activation, Acc. Chem. Res. 40 (2007) 543–553.
[19] J. Chlistunoff, RRDE and voltammetric study of ORR on pyrolyzed Fe/polyaniline catalyst. On the origins of variable Tafel slopes, J. Phys. Chem. C 115 (14) (2011) 6496–6507.
[20] A. Damjanovic, V. Brusic, Electrode kinetics of oxygen reduction on oxide-free platinum electrodes, Electrochim. Acta 12 (1967) 615–628.
[21] O. Antoine, Y. Bultel, R. Durand, Oxygen reduction reaction kinetics and mechanism on platinum nanoparticles inside Nafion®, J. Electroanal. Chem. 499 (2001) 85–94.
[22] O. Antoine, R. Durand, RRDE study of oxygen reduction on Pt nanoparticles inside Nafion: H_2O_2 production in PEMFC cathode conditions, J. Appl. Electrochem. 30 (2000) 839–844.
[23] Y. Garsany, O.A. Baturina, K.E. Swider-Lyons, S.S. Kocha, Experimental methods for quantifying electrocatalysts for the oxygen reduction reaction, Anal. Chem. 82 (2010) 6321–6328.
[24] H. Schulenburg, S. Stankov, V. Schünemann, J. Radnik, I. Dorbandt, S. Fiechter, P. Bogdanoff, H. Tributsch, Catalysts for the oxygen reduction from heat-treated iron(III) tetramethoxyphenylporphyrin chloride: structure and stability of active sites, J. Phys. Chem. B 107 (2003) 9034–9041.
[25] S. Liu, W. Bian, Z. Yang, J. Tian, C. Jin, M. Shen, Z. Zhou, R. Yang, A facile synthesis of $CoFe_2O_4$/biocarbon nanocomposites as efficient bi-functional electrocatalysts for the oxygen reduction and oxygen evolution reaction, J. Mater. Chem. A 2 (2014) 18012–18017.
[26] E.J. Coleman, M.H. Chowdhury, A.C. Co, Insights into the oxygen reduction reaction activity of Pt/C and PtCu/C catalysts, ACS Catal. 5 (2015) 1245–1253.
[27] A. Muthukrishnan, Y. Nabae, W.C. Chang, T. Okajima, T. Ohsaka, A high-performance Fe and nitrogen doped catalyst derived from diazoniapentaphene salt and phenolic resin mixture for oxygen reduction reaction, Catal. Sci. Technol. 5 (2015) 1764–1774.
[28] Y. Sun, J. Wu, J. Tian, C. Jin, R. Yang, Sulfur-doped carbon spheres as efficient metal-free electrocatalysts for oxygen reduction reaction, Electrochim. Acta 178 (2015) 806–812.
[29] G. Lu, Y. Zhu, K. Xu, Y. Jin, Z.J. Ren, Z. Liu, W. Zhang, Metallated porphyrin based porous organic polymers as efficient electrocatalysts, Nanoscale 7 (2015) 18271–18277.
[30] M. Lefevre, J.P. Dodelet, Molecular oxygen reduction in PEM fuel cells: evidence for the simultaneous presence of two active sites in Fe-based catalysts, J. Phys. Chem. B 106 (2002) 8705–8713.
[31] H. Iden, S. Takaichi, Y. Furuya, T. Mashio, Y. Ono, A. Ohma, Relationship between gas transport resistance in the catalyst layer and effective surface area of the catalyst, J. Electroanal. Chem. 694 (2013) 37–44.
[32] S. Beyhan, N.E. Sahin, S. Pronier, J.-M. Leger, F. Kadirgan, Comparison of oxygen reduction reaction on Pt/C, Pt-Sn/C, Pt-Ni/C, and Pt-Sn-Ni/C catalysts prepared by Bönnemann method: a rotating ring disk electrode study, Electrochim. Acta 151 (2015) 565–573.
[33] T. Mashio, K. Sato, A. Ohma, Analysis of water adsorption and condensation in catalyst layers for polymer electrolyte fuel cells, Electrochim. Acta 140 (2014) 238–249.
[34] S. Garcia-Rodriguez, S. Rojas, M. Vellosillo, M.A. Pena, J.L.G. Fierro, Role of perfluorosulfonic ionomer as protective agent against strong adsorption of (bi)sulfate anions. Relevance in the determination of the area of Pt/C electrocatalysts, Int. J. Hydrog. Energy 35 (2010) 11576–11581.
[35] K. Shinozaki, J.W. Zack, S. Pylypenko, B.S. Pivovar, S.S. Kocha, Oxygen reduction reaction measurements on platinum electrocatalysts utilizing rotating disk electrode technique II. Influence of ink formulation, catalyst layer uniformity and thickness, J. Electrochem. Soc. 162 (12) (2015) F1384.
[36] V. Freger, Hydration of ionomers and Schroeder's paradox in Nafion, J. Phys. Chem. B 113 (2009) 24–36.
[37] S. Ma, Q. Chen, F.H. Jøgensen, P.C. Stein, E.M. Skou, ^{19}F NMR studies of Nafion™ ionomer adsorption on PEMFC catalysts and supporting carbons, Solid State Ionics 178 (2007) 1568–1575.
[38] S. Ma Andersen, M. Borghei, R. Dhiman, H. Jiang, V. Ruiz, E. Kauppinen, E. Skou, Interaction of multi-walled carbon nanotubes with perfluorinated sulfonic acid ionomers and surface treatment studies, Carbon 71 (2014) 218–228.
[39] S. Ma Andersen, M. Borghei, R. Dhiman, V. Ruiz, E. Kauppinen, E. Skou, Adsorption behavior of perfluorinated sulfonic acid ionomer on highly graphitized carbon nanofibers and their thermal stabilities, J. Phys. Chem. C 118 (2014) 10814–10823.
[40] S. Ma Andersen, Nano carbon supported platinum catalyst interaction behavior with perfluorosulfonic acid ionomer and their interface structures, Appl. Catal. B Environ. 181 (2016) 146–155.

[41] O.V. Cherstiouk, P.A. Simonov, V.B. Fenelonov, E.R. Savinova, Influence of Nafion ionomer on carbon corrosion, J. Appl. Electrochem. 40 (2010) 1933–1939.
[42] J. Durst, A. Siebel, C. Simon, F. Hashe, J. Herranz, H.A. Gasteiger, New insights into the electrochemical hydrogen oxidation and evolution reaction mechanism, Energy Environ. Sci. 7 (2014) 2255–2260.
[43] J. Durst, C. Simon, F. Hashe, H.A. Gasteiger, Hydrogen oxidation and evolution reaction kinetics on carbon supported Pt, Ir, Rh, and Pd electrocatalysts in acidic media, J. Electrochem. Soc. 162 (1) (2015) F190–F203.
[44] K. Kinoshita, Carbon: Electrochemical and Physicochemical Properties, John Wiley & Sons, New York, NY, 1988.
[45] F. Hashe, M. Oezaslan, P. Strasser, Activity, stability and degradation of multi walled carbon nanotube (MWCNT) supported Pt fuel cell electrocatalysts, Phys. Chem. Chem. Phys. 12 (2010) 15251–15258.
[46] R. Guzman-Blas, D. Suazo-Davila, C.A. Velez, C.E. Daza, D.J. Stacchiola, K. Sasaki, S.D. Senanayake, A.C. Johnston-Peck, R. Molina, C.R. Cabrera, EDTA-Ce(III) modified Pt Vulcan XC-72 catalyst synthesis for methanol oxidation in acid solution, Electrocatalysis 5 (2014) 50–61.
[47] P. Scherrer, Bestimmung der Grösse und der inneren Struktur von Kolloidteilchen mittels Röntgenstrahlen, Nachr. Ges. Wissenschaften, Göttingen, 1918 98–100.
[48] J.O.M. Bockris, M.A.V. Devanathan, K. Müller, On the structure of charged interfaces, Proc. R. Soc. London, Ser. A 274 (1356) (1963) 55–79.
[49] I. Langmuir, The adsorption of gases on plane surfaces of glass, mica and platinum, J. Am. Chem. Soc. 40 (9) (1918) 1361–1403.
[50] M. Lopez-Haro, L. Guetaz, T. Printemps, A. Morin, S. Escribano, P.-H. Jouneau, P. Bayle-Guillemaud, F. Chandezon, G. Gebel, Three-dimensional analysis of Nafion layers in fuel cell electrodes, Nat. Commun. 5 (2014) 1–6.
[51] L. Castanheira, W.O. Silva, F.H.B. Lima, A. Crisci, L. Dubau, F. Maillard, Carbon corrosion in proton-exchange membrane fuel cells: effect of the carbon structure, the degradation protocol, and the gas atmosphere, ACS Catal. 5 (2015) 2184–2194.
[52] K. Artyushkova, S. Pylypenko, M. Dowlapalli, P. Atanassov, Structure-to-property relationships in fuel cell catalyst supports: correlation of surface chemistry and morphology with oxidation resistance of carbon blacks, J. Power Sources 214 (2012) 303–313.
[53] T. Mashio, K. Malek, M. Eikerling, A. Ohma, H. Kanesaka, K. Shinohara, Molecular dynamics study of ionomer and water adsorption at carbon support materials, J. Phys. Chem. C 114 (2010) 13739–13745.
[54] T. Masuda, H. Naohara, S. Takakusagi, P.R. Singh, K. Uosaki, Formation and structure of perfluorosulfonated ionomer thin film on a graphite surface, Chem. Lett. 38 (9) (2009) 884–885.
[55] P.J.F. Harris, Fullerene-related structure of commercial glassy carbons, Philos. Mag. 84 (29) (2004) 3159–3167.
[56] K.J.J. Mayrhofer, D. Strmcnik, B.B. Blizanac, V. Stamenkovic, M. Arenz, N.M. Markovic, Measurement of oxygen reduction activities via the rotating disc electrode method: from Pt model surfaces to carbon-supported high surface area catalysts, Electrochim. Acta 53 (2008) 3181–3188.
[57] A. Ohma, K. Fushinobu, K. Okazaki, Influence of Nafion® film on oxygen reduction reaction and hydrogen peroxide formation on Pt electrode for proton exchange membrane fuel cell, Electrochim. Acta 55 (2010) 8829–8838.
[58] Y. Garsany, I.L. Singer, K.E. Swider-Lyons, Impact of film drying procedures on RDE characterization of Pt/VC electrocatalysts, J. Electroanal. Chem. 662 (2011) 396–406.
[59] E. Guilminot, A. Corcella, M. Chatenet, F. Maillard, Comparing the thin-film rotating disk electrode and the ultramicroelectrode with cavity techniques to study carbon-supported platinum for proton exchange membrane fuel cell applications, J. Electroanal. Chem. 599 (2007) 111–120.
[60] J. Perez, E.R. Gonzalez, E.A. Ticianelli, Oxygen electrocatalysis on thin porous coating rotating platinum electrodes, Electrochim. Acta 44 (1998) 1329–1339.
[61] F. Gloaguen, P. Convert, S. Gamburzev, O.A. Velev, S. Srinivasan, An evaluation of the macro-homogeneous and agglomerate model for oxygen reduction in PEMFCs, Electrochim. Acta 43 (24) (1998) 3767–3772.
[62] M. Perry, J. Newman, E.J. Cairns, Mass transport in gas-diffusion electrodes: a diagnostic tool for fuel-cell cathodes, J. Electrochem. Soc. 145 (1) (1998) 5–15.
[63] P. Jiang, X. Ma, J. Ning, C. Song, X. Chen, J.-F. Jia, Q.-K. Xue, Quantum size effect directed selective self-assembling of cobalt phthalocyanine on Pb(111) thin films, J. Am. Chem. Soc. 130 (25) (2008) 7790–7791.
[64] B.R. Kozub, R.G. Compton, Voltammetric studies of the redox mediator, cobalt phthalocyanine, with regard to its claimed electrocatalytic properties, Sensors Actuators B 147 (2010) 350–358.
[65] J. Marie, R. Chenitz, M. Chatenet, S. Berthon-Fabry, N. Cornet, P. Achard, Highly porous PEM fuel cell cathodes based on low density carbon aerogels as Pt-support: experimental study of the mass-transport losses, J. Power Sources 190 (2009) 423–434.
[66] J. Katsounaros, W.B. Schneider, J.C. Meier, U. Benedikt, P.U. Biedermann, A. Cuesta, A.A. Auer, K.J.J. Mayrhofer, The impact of spectator species on the interaction of H_2O_2 with platinum – implications for the oxygen reduction reaction pathways, Phys. Chem. Chem. Phys. 15 (2013) 8058–8068.
[67] J. Chlistunoff, B. Pivovar, Effects of ionomer morphology on oxygen reduction on Pt, J. Electrochem. Soc. 162 (8) (2015) F890–F900.
[68] M. Uchida, Y. Fukuoka, Y. Sugawara, H. Ohara, A. Ohta, Improved preparation process of very-low-platinum-loading electrodes for polymer electrolyte fuel cells, J. Electrochem. Soc. 145 (11) (1998) 3708–3713.
[69] J. Marie, S. Berthon-Fabry, M. Chatenet, E. Chainet, R. Pirard, N. Cornet, P. Achard, Platinum supported on resorcinol–formaldehyde based carbon aerogels for PEMFC electrodes: influence of the carbon support on electrocatalytic properties, J. Appl. Electrochem. 37 (2007) 147–153.
[70] A.J. Bard, L.R. Faulkner, Electrochemical Methods: Fundamentals and Applications, 2nd ed. John Wiley & Sons, New York, Chichester, Weinheim, Brisbane, Singapore, Toronto, 2001.
[71] B. Chilukuri, U. Mazur, K.W. Hipps, Effect of dispersion on surface interactions of cobalt(II) octaethylporphyrin monolayer on Au(111) and HOPG(0001) substrates: a comparative first principles study, Phys. Chem. Chem. Phys. 16 (2014) 14096–14107.
[72] T.-T. Zhang, C.-J. Wang, K. Sun, H.-K. Yuan, J.-Z. Wang, Step-by-step self-assembly of manganese phthalocyanine on Bi(111) surface: from single molecule to two-dimensional domains, Appl. Surf. Sci. 317 (2014) 1047–1051.
[73] V. Feyer, M. Graus, P. Nigge, M. Wiessner, R.G. Acres, C. Wiemann, C.M. Schneider, A. Schöll, F. Reinert, Adsorption geometry and electronic structure of iron phthalocyanine on Ag surfaces: a LEED and photoelectron momentum mapping study, Surf. Sci. 621 (2014) 64–68.
[74] J. Lüder, O. Eriksson, B. Sanyal, B. Brena, Revisiting the adsorption of copper-phthalocyanine on Au(111) including van der Waals corrections, J. Chem. Phys. 140 (2014) 124711-1–124711-7.
[75] S.R. Wagner, P. Zhang, Formation of highly ordered organic molecular thin films on deactivated Si surfaces studied by scanning tunneling microscopy and low energy electron diffraction, J. Phys. Chem. C 118 (2014) 2194–2201.
[76] S.-B. Lei, S.-X. Yin, C. Wang, L.-J. Wan, C.-L. Bai, Selective adsorption of copper phthalocyanine atop functionalized organic monolayers, J. Phys. Chem. B 108 (2004) 224–227.
[77] P.i. Järvinen, S.K. Hämäläinen, M. Ijäs, A. Harju, P. Liljeroth, Self-assembly and orbital imaging of metal phthalocyanines on a graphene model surface, J. Phys. Chem. C 118 (2014) 13320–13325.
[78] X. Miao, A. Gao, S. Hiroto, H. Shinokubo, A. Osuka, H. Xin, W. Deng, Adsorption characteristic of self-assembled corrole dimers on HOPG, Surf. Interface Anal. 41 (2009) 225–230.
[79] Y. Chin, D. Panduwinata, M. Sintic, T.J. Sum, N.S. Hush, M.J. Crossley, J.R. Reimers, Atomic-resolution kinked structure of an alkylporphyrin on highly ordered pyrolytic graphite, J. Phys. Chem. Lett. 2 (2011) 62–66.
[80] Q. Ferreira, A.M. Braganca, N.M.M. Moura, M.A.F. Faustino, R. Alcacer, J. Morgado, Dynamics of porphyrin adsorption on highly oriented pyrolytic graphite monitored by scanning tunnelling microscopy at the liquid/solid interface, Appl. Surf. Sci. 273 (2013) 220–225.
[81] S.K. Hämäläinen, M. Stepanova, R. Drost, P. Liljeroth, J. Lahtinen, J. Sainio, Self-assembly of cobalt-phthalocyanine molecules on epitaxial graphene on Ir(111), J. Phys. Chem. C 116 (2012) 20433–20437.
[82] M. Scarselli, P. Castrucci, D. Monti, M. De Crescenzi, Studies of the adsorption of tetraphenylporphyrin molecules on graphite, Surf. Sci. 601 (2007) 5526–5532.
[83] T. Soboleva, X. Zhao, K. Malek, Z. Xie, T. Navessin, S. Holdcroft, On the micro-, meso-, and macroporous structures of polymer electrolyte membrane fuel cell catalyst layers, ACS Appl. Mater. Interfaces 2 (2) (2010) 375–384.
[84] M. Uchida, Y. Fukuoka, Y. Sugawara, N. Eda, A. Ohta, Effects of microstructure of carbon support in the catalyst layer on the performance of polymer-electrolyte fuel cells, J. Electrochem. Soc. 143 (7) (1996) 2245–2252.
[85] J. Chlistunoff, J.-M. Sansiñena, Effects of axial coordination of the metal center on the activity of iron tetraphenylporphyrin as a nonprecious catalyst for oxygen reduction, J. Phys. Chem. C 118 (2014) 19139–19149.